

Production of Biodiesel and Ethanol from Algae

A Technical Report
presented to the faculty of the
School of Engineering and Applied Science
University of Virginia

by

Schuyler Dineen
Jack Pagan
Michael Schapowal
Amna Tahir
David Vann

April 7, 2020

On my honor as a University student, I have neither given nor received unauthorized aid on this assignment as defined by the Honor Guidelines for Thesis-Related Assignments.

Signed: _____

Approved: _____ Date _____
Eric Anderson, Department of Chemical Engineering

Table of Contents

Body of Report

Summary	7
1. Introduction	9
2. Previous Work	11
3. Discussion	15
3.1 Algae Cultivation and Harvesting	15
3.1.1 Algae Strain	15
3.1.2 Algae Growth	15
3.1.3. Growth Conditions	17
3.1.4 Raceway Design Considerations	22
3.1.5 Algae Harvesting	24
3.1.6 Flocculation	25
3.1.7 Sedimentation	27
3.2 Algae Pretreatment	29
3.3 Lipid Extraction	31
3.3.1 Lipid Separation with Hexane	31
3.3.2 Hexane Recovery	33
3.4. Biodiesel Production and Purification	34
3.4.1 Supercritical Transesterification of Algal Oil to Fatty Acid Ethyl Esters (FAEEs/Biodiesel)	35
3.4.2 Product Separation and Purification of Biodiesel	37
3.5 Fermentation Pretreatment	40
3.5.1 Neutralization	40
3.5.2 Evaporation	41
3.5.3 Rotary Vacuum Drum Filtration	43
3.6 Fermentation and Ethanol Purification	45
3.6.1 Continuous Fermentation	45
3.6.2 Solids Separation	46
3.6.3 Distillation to Azeotrope	47
3.6.4 Azeotrope Breaking	48
4. Recommended Design	50
4.1 Algae Cultivation and Harvesting	50
4.1.1 Algae Cultivation	50

4.1.2 Algae Harvesting	51
4.2 Algae Pretreatment	54
4.3 Lipid Extraction	57
4.3.1 Lipid Separation with Hexane	57
4.3.2 Hexane Recovery	59
4.4 Biodiesel Production and Purification	63
4.4.1 Transesterification Reactor	63
4.4.2 Ethanol Separation and Recycle	64
4.4.3 Biodiesel Purification	66
4.4.4 Ancillary Equipment	69
4.5 Fermentation Pretreatment	71
4.5.1 Neutralization	73
4.5.2 Evaporation	75
4.5.3 Rotary Vacuum Drum Filtration	76
4.6 Fermentation and Ethanol Purification	78
4.6.1 Continuous Fermentation	78
4.6.2 Solids Separation	80
4.6.3 Distillation to Azeotrope	81
4.6.4 Azeotrope Breaking	83
5. Economic Analysis	86
5.1 Equipment Purchase and Operating Costs	86
5.1.1 Algae Cultivation and Harvesting	86
5.1.2 Algae Pretreatment	90
5.1.3 Lipid Extraction	92
5.1.4 Biodiesel Production and Purification	94
5.1.5 Fermentation Pretreatment	97
5.1.6 Fermentation and Ethanol Purification	99
5.2 Total Capital and Operating Costs	101
5.2.1 Fixed Capital Costs	101
5.2.2 Working and Total Capital Costs	102
5.2.3 Operating Cost and Product Revenue	103
5.2.4 Labor Costs	105
5.2.5 Taxes and Other Fees	106
5.2.6 Cash Flow Analysis	107
5.3 Scenarios	109
5.3.1 Increased Fuel Prices	109
5.3.2 Better Algae Growth	110

5.3.3 Multiple Effect Evaporation	110
5.3.4 Glycerol and Gypsum Side Products	112
5.3.5 Avoiding Neutralization and Evaporation	113
5.3.6 Eliminating Ethanol Production	115
6. Safety, Health, Environmental, and Social Considerations	118
6.1 Health and Safety Considerations	118
6.2 Environmental Considerations	119
6.3 Social Considerations	122
7. Conclusions and Recommendations	123
8. Acknowledgements	125
9. References	126

Figures

Figure 0-0-01: Block Flow Diagram of Biofuel Refinery	8
Figure 3-1-01: Chlorella Vulgaris Growth Profiles	16
Figure 3-1-02: Maximum Light Intensity and Temperature	18
Figure 3-1-03: High and low temperatures in Houston, Texas	18
Figure 3-1-04: Light intensity in Houston, Texas	19
Figure 3-1-05: pH of Raceways	20
Figure 3-1-06: Layout of Each Open Pond Raceway	23
Figure 3-1-07: General Raceway Layout	24
Figure 3-1-08: Settling velocity and concentration factor vs. shear force	26
Figure 3-3-01: Triolein Molecule	31
Figure 3-4-01: Transesterification Reaction	35
Figure 3-6-01: Zeolite Mass versus Ethanol Concentration	49
Figure 4-1-01: Algae Cultivation and Harvesting Process Flow Diagram	50
Figure 4-2-01: Algae Pretreatment Process Flow Diagram	54
Figure 4-3-01: Lipid Separation and Hexane Recovery Process Flow Diagram	57
Figure 4-4-01: Biodiesel Production and Purification Process Flow Diagram	63
Figure 4-5-01: Fermentation Pretreatment Process Flow Diagram	71
Figure 4-6-01: Continuous Fermentation Process Flow Diagram	78
Figure 4-6-02: Decanter Centrifuges Process Flow Diagram	80
Figure 4-6-03: Ethanol Distillation Process Flow Diagram	82
Figure 4-6-04: Azeotrope Breaking Process Flow Diagram	83
Figure 5-2-01: Cumulative Discounted Cash Flow	108
Figure 5-3-01: Cumulative Discounted Cash Flow at Higher Fuel Prices	109

Tables

Table 4-1-01: Raceway R-101 Specifications	51
Table 4-1-02: Algae Cultivation Pump Specifications	51
Table 4-1-03: Mixer M-101 Specifications	51
Table 4-1-04: Sedimentation Tank R-102 Specifications	52
Table 4-1-05: Algae Harvesting Pump Specifications	52
Table 4-1-06: Algae Cultivation and Harvesting Balances	53
Table 4-2-01: Algae Pretreatment Mass Flows	55
Table 4-2-02: Algae Pretreatment Equipment Specifications	56
Table 4-3-01: Mass Balance around S-301A/B	60
Table 4-3-02: Mass Balance Around E-301	60
Table 4-3-03: Lipid Extraction and Algae Recovery Equipment Specifications	61
Table 4-4-01: Transesterification Reactor R-401 Mass Flows	64
Table 4-4-02: Transesterification Reactor R-401 Specifications	64
Table 4-4-03: Ethanol Separation Column T-401 Mass Flows	65
Table 4-4-04: Ethanol Separation Column T-401 Specifications	65
Table 4-4-05: Ethanol Separation Column Condenser E-403 and Reboiler E-404	65
Table 4-4-06: Two-phase Settler S-401 Mass Flows	67
Table 4-4-07: Two-phase Gravity Settler S-401 Specifications	67
Table 4-4-08: Secondary Flash Drum S-402 Mass Flows	67
Table 4-4-09: Secondary Flash Drum S-402 Specifications	68
Table 4-4-10: Biodiesel Purification Column T-402 Mass Flows	68
Table 4-4-11: Biodiesel Purification Column T-402 Specifications	68
Table 4-4-12: Biodiesel Purification Column Condenser E-406 and Reboiler E-407	68
Table 4-4-13: Biodiesel Heat Exchangers	69
Table 4-4-14: Biodiesel Pumps	70
Table 4-4-15: Fired Heater	70
Table 4-5-01: Fermentation Pretreatment Equipment Specifications	72
Table 4-5-02: Neutralization Mass Flows	73
Table 4-5-03: Neutralization Reactor R-501A/B Specifications	74
Table 4-5-04: Evaporation Mass Flows	75
Table 4-5-05: Rotary Vacuum Drum Filtration Mass Flows	76
Table 4-5-06: Rotary Vacuum Drum Filtration F-501A/AI Specifications	77
Table 4-6-01: Continuous Fermentation Mass Flows	79
Table 4-6-02: Continuous Fermentation Specifications	79
Table 4-6-03: Solids Separation Mass Flows	81
Table 4-6-04: Solids Separation Specifications	81
Table 4-6-05: Azeotropic Distillation Mass Flows	82
Table 4-6-06: Azeotropic Distillation Specifications	82

Table 4-6-07: Azeotropic Breaking Mass Flows	84
Table 4-6-08: Azeotropic Breaking Specifications	84
Table 4-6-09: Ethanol Production Ancillary Equipment Specifications	85
Table 5-1-01: Cost of Land	86
Table 5-1-02: Cost of Building Raceways	87
Table 5-1-03: Cost of PVC Liner	87
Table 5-1-04: Purchased Equipment Pricing of Algae Cultivation	88
Table 5-1-05: Purchased Equipment Cost of Sedimentation Tanks	88
Table 5-1-06: Operating Cost of Algae Cultivation and Harvesting	89
Table 5-1-07: Purchased Equipment Cost for Algae Pretreatment	90
Table 5-1-08: Operating Costs for Algae Pretreatment	91
Table 5-1-09: Purchased Equipment Costs and Initial Material Cost for Lipid Extraction	92
Table 5-1-10: Operating Costs for Lipid Extraction	93
Table 5-1-11: Purchased Equipment Cost for Biodiesel Production and Purification	94
Table 5-1-12: Operating Costs for Biodiesel Production and Purification	96
Table 5-1-13: Purchased Equipment Cost for Fermentation Pretreatment	97
Table 5-1-14: Operating Costs for Fermentation Pretreatment	98
Table 5-1-15: Purchased Equipment Cost for Ethanol Fermentation and Purification	99
Table 5-1-16: Operating Costs for Ethanol Production	100
Table 5-2-01: Factors to Estimate Fixed Capital Cost from Purchased Equipment Cost	101
Table 5-2-02: Estimation of Capital Cost from Purchased Equipment Cost	102
Table 5-2-03: Summary of Total Capital Costs	103
Table 5-2-04: Operating Costs Summary	103
Table 5-2-05: Product Revenue	104
Table 5-2-06: Number of Process Steps	105
Table 5-2-07: Labor Costs	106
Table 5-2-08: Operating Cash Flow	107
Table 5-3-01: Number of Evaporator Effects Return on Investment	111
Table 5-3-02: Product Revenue with Side Products	112
Table 5-3-03: Change in Total Capital Costs in Solid Acid Catalyst Scenario	114
Table 5-3-04: Change in Operating Costs with Solid Acid Catalyst Scenario	115
Table 5-3-05: Change in Total Capital Costs with Ethanol Elimination	116
Table 5-3-06: Change in Operating Costs with Ethanol Elimination	116

Summary

Biofuels provide a green alternative to fossil fuels, however current biofuels increase food prices, compete with food crops for land, or are prohibitively expensive. Algal biofuels do not compete with food crops, but attempts to produce biodiesel or ethanol from algae have been uneconomical. Coproduction of biodiesel and ethanol could prove profitable. To investigate, we designed an algae farm and biorefinery using kinetic data from literature, physical modeling with Aspen Plus, and mass and heat transfer fundamentals. Economic analysis was performed based on equipment pricing as well as input and output, utility, labor, taxes, and insurance costs.

This process begins with municipal wastewater which is introduced into algal cultivation raceways. The algae is allowed to grow for 14 days before being concentrated through sedimentation. Sulfuric acid disrupts the algae, producing glucose and freeing the lipids. The lipids are extracted with hexane and transesterified to biodiesel with supercritical ethanol. The biodiesel is purified with distillation and phase separation between glycerol and biodiesel. From lipid extraction, the sugar and algae stream is neutralized with calcium hydroxide, evaporated to concentrate glucose, and filtered to remove calcium sulfate. Continuous yeast fermentation produces ethanol from glucose. Centrifuges remove remaining solids, and ethanol is purified by distillation with zeolite adsorption to break the azeotrope. A quarter of the ethanol is recycled to transesterification. Figure 0-0-01 summarizes the process.

The final design for the plant produces 6.1M gallons of biodiesel and 3.9M gallons of ethanol per year. As designed, the plant costs \$513,584,000 in capital and loses \$95,332,000 per year. The plant would be worth investment at prices of \$5.35/gallon of ethanol and \$21.39/gallon of biodiesel, although design changes could reduce this to \$2.88/gallon ethanol and

\$11.53/gallon biodiesel. The plant consumes more energy than it produces. The process still results in net carbon dioxide sink and also removes nitrogen from wastewater, something that wastewater facilities have trouble dealing with. A significant amount of land and water must be processed in order to produce 220 tons/algae a day. Processing and removing such large quantities of water results in large power requirements and costs. Better algae strains and cultivation technology is needed to make algal biofuels viable.

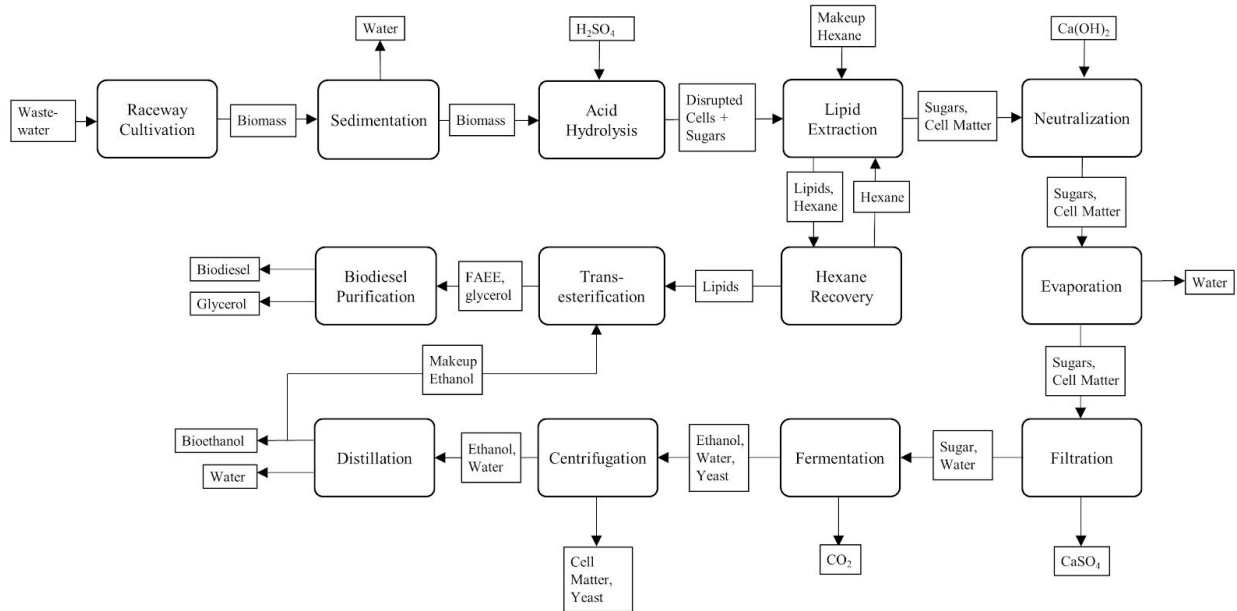


Figure 0-0-01: Block Flow Diagram of Biofuel Refinery

1. Introduction

For as long as the world has used energy, the production goals have been maximizing cost effectiveness and efficiency. However, as the drilling for oil continues to increase, it is inevitable that we will lose our traditional oil reserves by 2050 (De Bhowmick et al., 2019). There is no simple solution to a rising energy demand and nonrenewable sources. Providing alternative liquid fuels is one solution that has seen increasing interest in the last few decades. Reforms in the transport sector policy have made biofuels tremendously more reasonable to produce (Gnansounou & Kenthorai Raman, 2016). This world dominated by fossil fuel has adverse effects on the environment: global warming and weather extremes are all worsened by greenhouse gases (De Bhowmick et al., 2019). It was only in the past few decades that environmental impact and sustainability became pressing issues for the public. Global warming is a rising concern with impacts including but not limited to extreme weather conditions and sea level rise (Gnansounou & Kenthorai Raman, 2016). Increase in fossil fuel use results in high carbon dioxide emissions and contributes significantly to global warming. In an attempt to mitigate the effects, renewable technology industries have seen increased research as well as production.

In the United States today, bioethanol, primarily from corn, and biodiesel, primarily from soybean and rapeseed (canola) oil, are the most common biofuels in use, accounting for 16.1 billion gallons of ethanol (~10% of current motor fuel usage) and 1.83 billion gallons of biodiesel in 2018 (U.S. Energy Information Administration, 2019b). Biofuels produced from algae represent a potentially significant advancement to presently commercialized biofuels. Algae grow quickly, can be rich in oil, and are currently the only biofuel source technically

capable of meeting more than half of U.S. fuel usage, as traditional biofuels require large amounts of land (Chisti, 2007). In addition to lower land usage, algal biofuels do not compete with food for land - a concern with current biofuels (Ajanovic, 2011)- since they can be grown in a wide variety of conditions and can be easily modified through genetic engineering for different strain characteristics (Gomiero, 2015; Hannon et al., 2010).

2. Previous Work

The algae that is selected for biodiesel production must have two primary characteristics to make them favorable: they must grow quickly and produce a high lipid fraction. Additionally, wild type algae are desired so that they can thrive in an exposed outdoor environment. Some common examples of algae used in biodiesel production include *Chlorella vulgaris*, *Ochromonas danica*, and *Scenedesmus* sp. (Tripathi et al., 2019). It is typical to see large-scale algae facilities using raceways, which are large pools with agitators to circulate. These water tracks are outdoors so they can be exposed to sunlight but this can also introduce wild algae strains. For this reason it is best to start with wild algae so that it is not overrun as time passes.

There are many ways to extract the oils from these algae once they have completed their growth. Park explores a comparison of several of these methods including electroflotation with alternating current, pulsed electric fields, and hot water with sulfuric acid. These methods all were able to extract around 30 percent of the algae's weight in lipids (Park et al., 2015). After the extraction the algae cell mass is considered a waste stream and is discarded while the lipids are moved along for processing.

The lipids produced from the algae have need to be transesterified to make biodiesel. This process takes the long chains of a triglyceride and detaches them from their backbone. The carbon chains can be effectively used as a fuel source when the glycerol is removed. Park explores a myriad of methods to accomplish this mechanism; the most popular is the addition of a strong acid, but new methods such as supercritical baths of water and ethanol are being explored as an alternative means of getting the same result (Park et al., 2014). The supercritical method does not require the addition of a catalyst, as the other processes do.

From this point the biodiesel can be refined to make it fuel grade at an ester content of 96.5% (Jääskeläinen, 2009). Once the fuel is at this specification it can be sold and used in standard diesel engines. This seamless integration of the fuel is what makes biodiesel such a marketable technology.

Ethanol production is a biological process that occurs when plants are exposed to low oxygen environments and simple sugars. This process can be exploited for biofuel production because alcohol, namely ethanol, is a common fuel additive to gasoline or even a stand alone fuel. This production occurs at an industrial scale largely with corn sugars. However, ethanol can be produced with other higher energy density feedstocks than simple sugar, like cellulose. Fermentation is done in almost every application with simple yeast strains like *saccharomyces cerevisiae*, but can also be accomplished with certain strains of bacteria.

Several approaches have been developed to commercialize algal biodiesel, but there have been difficulties in algal cultivation that have hindered attempts to do so. In growing algae, open ponds and closed photobioreactors have been used. Open systems are cheaper, but are difficult to control, vulnerable to contamination, and can have issues with light penetration for photosynthesis (Saad et al., 2019). Closed systems give higher yields, are controllable, and save water, but are expensive and difficult to scale up (Saad et al., 2019). One company, Solazyme (now defunct), attempted to get around the issue of light penetration by engineering its algae to produce oil using a sugar substrate, allowing its algae to grow without sunlight in industrial fermenters (Biello, 2013); however, this approach is highly dependent on the price of sugar, and the use of sugar conflicts with avoiding competition with food and increases the environmental impact of the process. For photosynthetic algae, however, the limits of light penetration can

cause low cell density in cultivation, leading to lower production than theoretically possible, though still much higher than from typical agricultural sources (e.g., soybeans) (Dassey & Theegala, 2013; Li et al., 2008). Low cell densities, combined with the small size of algal cells and the high water content of algal biomass, make harvesting and drying algae costly (Li et al., 2008). While there are other costs associated with the production of biodiesel and other products, these are not unique to algae and are not as great a challenge as scaling up the growth of algae.

Ultimately, the high cost of cultivation and harvesting makes a biodiesel-only approach economically unfeasible. A fairly recent economic analysis of algal biodiesel production found a selling price of \$8.52/gallon was needed for an acceptable rate of return (Davis et al., 2011). Given that the current average petroleum diesel price in the U.S. is \$3.05/gallon (U.S. Energy Information Administration, 2019c), algal biodiesel is not economically competitive with fossil fuels on its own.

An interesting connection that can be made between the previously discussed technology is the unused cell mass from the algal biodiesel. This waste stream has potential as the feedstock for cellulosic ethanol. By combining these two processes, the entire facility can be made more profitable. The utilization of what would otherwise be a waste stream increases the production of high value products from the facility and increases revenue.

Martin recognized this potential and explored a theoretical facility which accomplishes both biodiesel production and ethanol production from a single algae source. The process begins in the same way biodiesel production does, with a separation of the oils from the cell mass (Martin & Grossmann, 2013). The cell mass is processed to starch, sugar, and eventually ethanol by the same process as standard ethanol production. The oils are transesterified and made into

biodiesel following a similar pathway to what was discussed above. Martin notes that this process has a slightly more selective process for the algae strain than for the other processes. The starch to oil ratio produced by the cells is critical because if it is weighted too far to one side, then either ethanol or diesel production will suffer (Martín & Grossmann, 2013). This facility structure and like papers form the foundation of our design for algal biodiesel and bioethanol production.

3. Discussion

3.1 *Algae Cultivation and Harvesting*

The purpose of algae cultivation is to produce algal biomass and lipids. Secondary wastewater will be used for nutrients essential for algal growth, such as nitrogen and phosphorus.

3.1.1 *Algae Strain*

A variety of different algae strains are available and can be used for biomass cultivation. We chose *Chlorella vulgaris* for our biorefinery as there is an abundance of kinetic data available for this strain. Further, *Chlorella vulgaris* has the capacity to produce large amounts of lipids in batch mode, while also demonstrating short biomass doubling times (Přibyl et al., 2012).

3.1.2 *Algae Growth*

We will be utilizing open pond raceways, as opposed to photobioreactors (PBR) since open pond raceways are much cheaper to construct and operate, though they do result in issues such as lower biomass densities, carbon dioxide and nutrient transfer limitations, and risk of contamination by other algae strains or bacteria (Saad et al., 2019). These open pond raceways will be operated in batch mode, allowing for nitrogen depletion to occur. In nitrogen depleted environments, microalgae can accumulate substantial amounts of neutral lipids, predominantly TAGs, which are desired in biofuel production (Přibyl et al., 2012).

Algae cultivation will be modeled after the cultivation regimes adopted by Amini et al. (2016, 2018) in their studies. In their study on cell harvesting density, environmental factors and medium depth, Amini et al. (2016) found that peak algal productivity in swine water was 80

tons/hectare/year while harvesting the algae at 0.1 g/L density and pond depth was 30 cm (Amini et al., 2016). However, when the cell harvesting density was increased to 0.4 g/L, the annual productivity was also much lower for higher harvesting cell density, at only 15 t/ha/year. Further, deeper raceways had a higher annual productivity at lower cell harvesting densities but at higher cell harvesting densities, steeper raceways performed better. This suggests that light attenuation deeper into the raceways is not a problem at low cell harvesting densities, around 0.1 g/L. This study highlights problems such as light attenuation and suggests that a lower harvesting density is ideal, especially to maximize areal biomass productivity (Amini et al., 2016). However, a limitation of this study is that harvesting cycle times and kinetics are not reported, and thus another study by Amini et al. using a similar set up and environmental factors was utilized in addition to this one.

In their study comparing harvesting cycle times, Amini et al. (2018) found that increasing algal growth periods resulted in decreased biomass productivities. They tested batch harvesting cycles of 3, 5 and 10 days and found the following growth profiles:

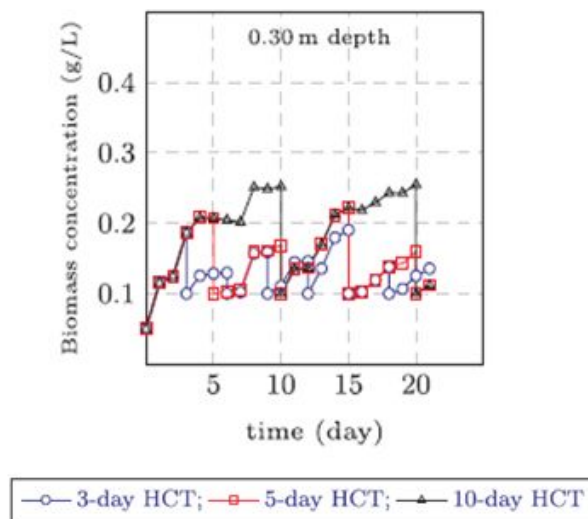


Figure 3-1-01: *Chlorella vulgaris* Growth Profiles (Amini et al., 2018)

Overall, it was found that the longer the cultivation time, the lower the overall biomass productivity, with a 3-day harvesting cycle resulting in the highest biomass productivity. However, a longer harvesting cycle is needed to allow the algae to utilize all the nitrogen present in the wastewater and result in nutrient depleted conditions (Amini et al., 2018). A harvesting cycle of 7 days was chosen, giving a harvesting biomass concentration of approximately 0.22 g/L. The biomass productivity of algae in this regime will be 68.25 tons/hectare/year.

We will be leaving 10% of the algae wastewater in the raceway as inoculum. It is worth noting that Amini et al.'s set up for harvesting was to leave 0.1 g/L of algae in raceways as inoculum. We are assuming that changing the amount of inoculum to 10% of the total growth, 0.02 g/L, instead of 0.1 g/L will not affect the final biomass concentration, due to the reduced light attenuation in the pond suggested by the study mentioned earlier. This assumption should be tested before implementation.

3.1.3. Growth Conditions

To ensure abundant algae growth, testing conditions, such as light intensity, temperature, and pH should be monitored and maintained close to either the conditions reported by Amini et al. or to the optimum for algal growth. The optimum temperature range for growth of *Chlorella vulgaris* is believed to be in the 20 – 30 C range, with temperatures above 35 C being detrimental to algal growth (Converti et al., 2009)

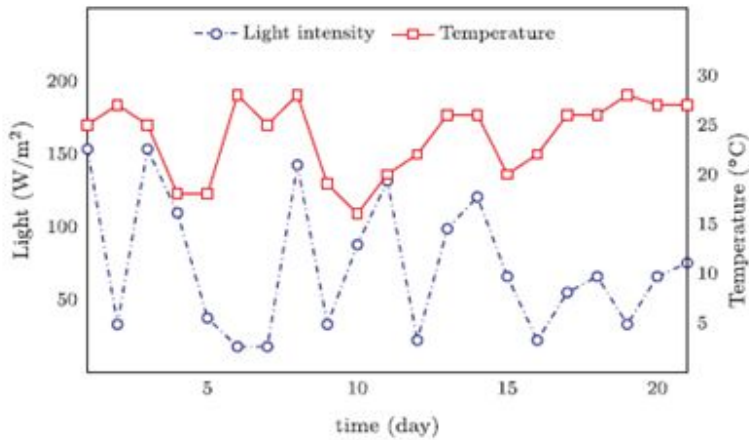


Figure 3-1-02: Maximum light intensity and temperature (Amini et al, 2018)

As can be seen in Figure 3-1-02, the outside temperature under which the results were achieved, ranges mostly in the 20 - 30 C optimum range, with a few dips below 20 C. Figure 3-1-03 depicts the high and low temperatures of Houston, Texas over the year. There is a large span over which the temperature remains in the optimum range, leading to a wide window for optimal performance. The temperature also peaks around August, reaching a high of 35 C. As this is the highest air temperature, the wastewater is expected to stay below this temperature.

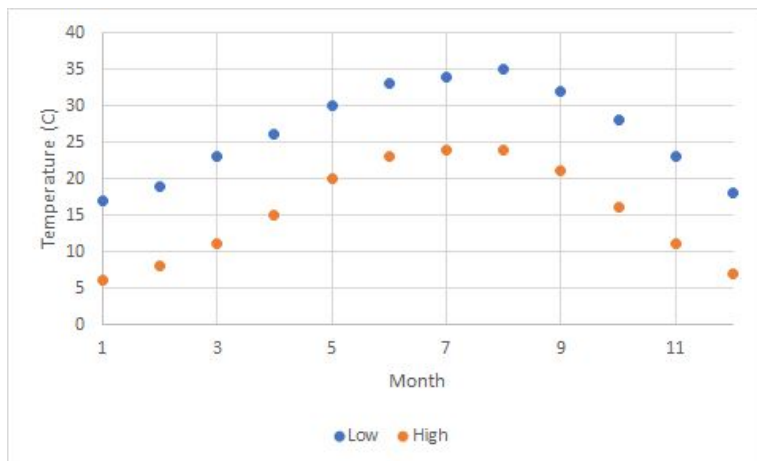


Figure 3-1-03: High and low temperatures in Houston, Texas (Houston TX Average

Temperatures by Month - Current Results, n.d.)

The optimal light intensity for algal growth is 200 $\mu\text{mol photons/m/s}$, or around 70 W/m^2 (Amini et al., 2016). As can be seen from Figure 3-1-02, the light intensity in Amini's study was consistently greater than the optimal amount, ranging between 125 and 175 W/m^2 . Further, the light intensity in Houston is also above the optimal 70 W/m^2 (Figure 3-1-04). While receiving higher than optimal amounts of light can lead to photoinhibition in algal growth, many models suggest that this photoinhibition plateaus once past a high enough light intensity (Dauta et al., 1990). This suggests that since the model conditions are already much higher than the optimal light intensity, the increased light intensity in Houston will not negatively impact algal growth any further.

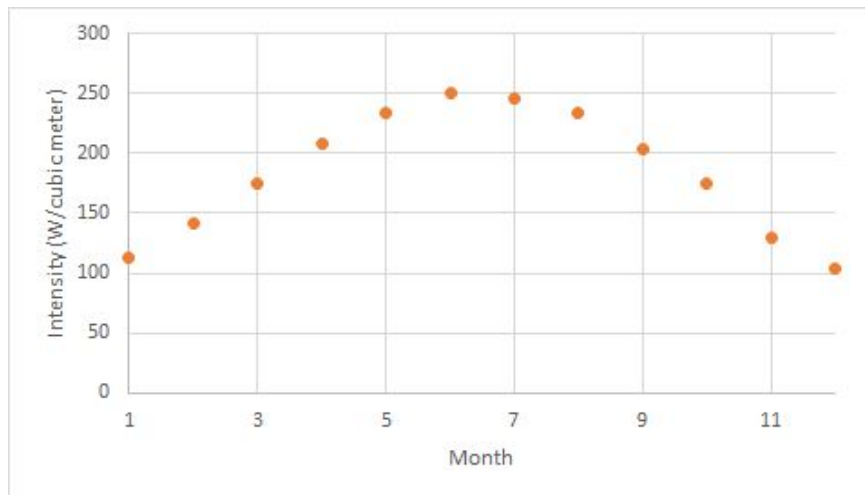


Figure 3-1-04: Light intensity in Houston, Texas (National Renewable Energy Laboratory)

This also suggests that the peak productivity variations over the year is more so a function of temperature than light intensity. We are assuming that algae production will operate at peak productivity through April - October, and at 50% productivity through November - March, based off of the temperature profile of Houston. The assumption should be tested prior to implementation of the refinery design.

Another important factor to consider is the pH of growth media. As carbon dioxide is consumed in the raceway, pH tends to decrease. Generally, carbon dioxide is pumped through the medium occasionally to lower the pH and help algae growth, as the optimum pH for algae growth is around 7.4 (Amini et al., 2016). In their study, Amini et al. (2018) did not add any additional carbon dioxide or air to their raceways. Figure 3-1-05 shows that over 7 days, the pH of the raceway increased from around 7.1 to 8.1. Following this study, we will not be pumping carbon dioxide or air through our system, but as a future improvement or study, recommend looking into how this design could be improved with the addition of carbon dioxide pumping. (Amini et al., 2018)

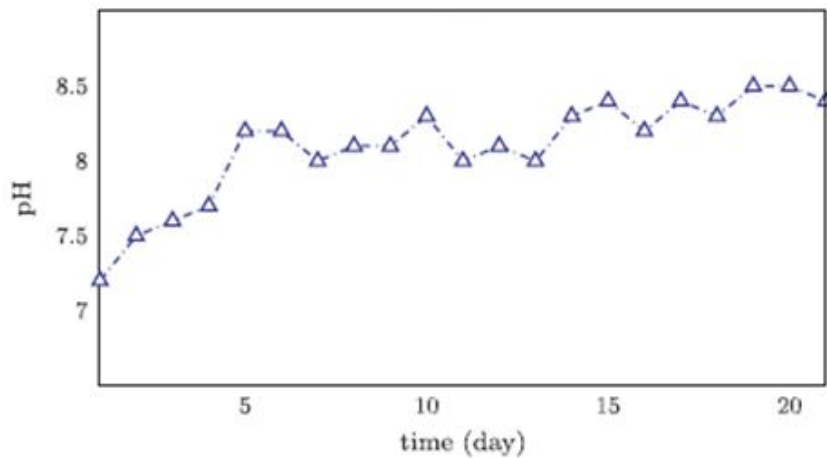


Figure 3-1-05: pH of raceways (Amini et al., 2018)

Lastly, it is worth noting that a higher concentration of nitrogen than available in our wastewater was utilized in the study used for reference. Nitrogen available in wastewater in municipal wastewater is around 51 mg/L (Woertz I. et al., 2009). However, algae growth was facilitated by Bold's medium in the base study, which has around 250 mg/L, and in the study

utilizing swine wastewater, which resulted in similar productivities, the nitrogen content was 102 mg/L (Amini et al., 2016; Amini et al., 2018).

Although the amount of incoming nitrogen is less concentrated than optimal, a sufficient total amount of nitrogen is available in the incoming wastewater. *Chlorella vulgaris* consists of around 5.6% of elemental nitrogen (Vassilev & Vassileva, 2016). In order to produce 220 tons of algae per day, 12.32 tons of nitrogen is thus needed. In the incoming 250 MGD of wastewater, assuming 51 mg/L of nitrogen in the wastewater, 48 tons of nitrogen is available. This suggests that the wastewater has enough nitrogen to sustain the growth of algae at estimated levels. However, the nitrogen content analysis of the specific wastewater should be done in order to ensure that the nitrogen level is as high as that found by Woertz (2008).

Further, Amini et al. found that the nutrient concentration of wastewater was depleted by 99.6% by the end of a ten day cultivation period (Amini et al., 2016). Other researchers have found varying nitrogen depletion abilities for algae. For example, Woertz et al. found that algae growth depleted 88% of nitrogen by day 15 while Mujtaba et al. (2012) found that algae was able to deplete more than 90% of the nitrogen in 7 days (Mujtaba et al., 2012; Woertz I. et al., 2009). While our cultivation period is only 7 days, most of the nitrogen will likely be depleted looking at the growth curves, as the growth slows down significantly by day 5. This suggests a lack of nutrients, namely nitrogen, and that the algae will be growing in nitrogen depleted conditions.

Finally, it is worth noting that around 5% of the growth media will consist of recycled wastewater as the wastewater capacity of Texas is not large enough to produce 220 tons/algae per day at the current conditions otherwise. Ferric chloride is not toxic to algae and is not

expected to hinder algae growth, especially as it is only around 0.00001% solid. This assumption should be tested before this plant is designed.

3.1.4 Raceway Design Considerations

Industrial algal raceways are generally large, spanning around a hectare or more of land, due to the large amounts of biomass desired for biofuel production. However, a study by Sutherland et al. (2020) shows that smaller raceways allow for higher algal areal productivities and improved nutrient depletion, suggesting that the optimum size for raceways is much smaller than the industrial size utilized today (Sutherland et al., 2020). The length to width ratio of raceways should be greater than 10 as a ratio smaller than that results in the flow in the straight part of the raceway to be affected by the disturbances caused at the bends (Chisti, 2016).

Keeping these considerations in mind, each raceway will be 100m x 20m wide, as can be seen in Figure 3-1-06.

As was seen in the study by Amini et al. (2016) earlier, shallower raceways are typically better as light attenuation can render the bottom of the raceways to go unused. However, when algae density is low, deeper ponds are desired as they can be fully utilized. Further, in another study, Sutherland found that biomass productivity and nutrient removal are both improved in 40 cm raceway, as opposed to 30 cm deep raceway (Sutherland et al., 2014). We will be utilizing a 40 cm deep pond considering the low final cell harvesting density and the desire for nitrogen depletion by the end of the 7 day cycle.

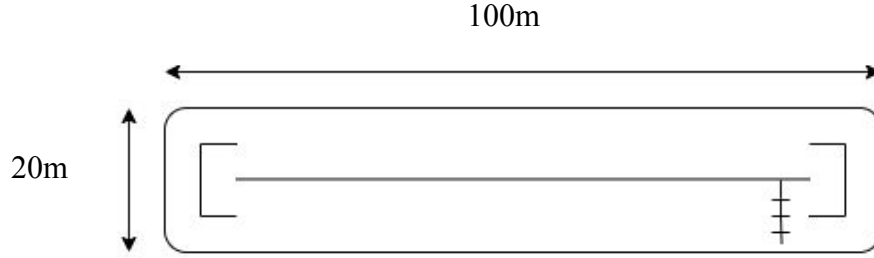


Figure 3-1-06: Layout of each open pond raceway

Open pond raceways often utilize a paddlewheel in order to facilitate mixing and minimize dead zones that tend to form near the bend of the raceway. The linear velocity of the pond is generally kept between 0.2 m/s to 0.3 m/s (Chisti, 2016). The linear velocity of the ponds will be kept at 0.2 m/s in order to minimize cell sedimentation (Amini et al., 2016). The flow in a raceway needs to be turbulent to ensure cell suspension, enhance vertical mixing, prevent thermal stratification, and facilitate removal of the oxygen generated by photosynthesis (Christi, 2016). A Reynolds number of 8000 and above is generally taken to indicate a turbulent regime in raceways. The Reynolds number was calculated to be approximately 98,000, well above the turbulent threshold, using the following equation (Christi, 2016):

$$Re = \frac{\rho u d_h}{\mu}$$

where d_h is defined as:

$$d_h = \frac{4wh}{w + 2h}$$

Power requirement is calculated using the following equation (Chisti, 2013):

$$P = \frac{1.59A\rho g u^3 f_M^2}{e d_h^{0.33}}$$

where d_h is the hydraulic diameter defined as above, f_M is the Manning channel roughness factor, and e is the efficiency of the paddlewheel, drive and motor. The value of f_M used was 0.012 s $m^{-1/3}$, which is typical for compacted gravel lined with a polymer membrane (Chisti 2013). The e

value is about 0.17 for a 8 impellers paddlewheel located in a channel. The power required per raceway is 195 W, and for all raceways is 1534 kW.

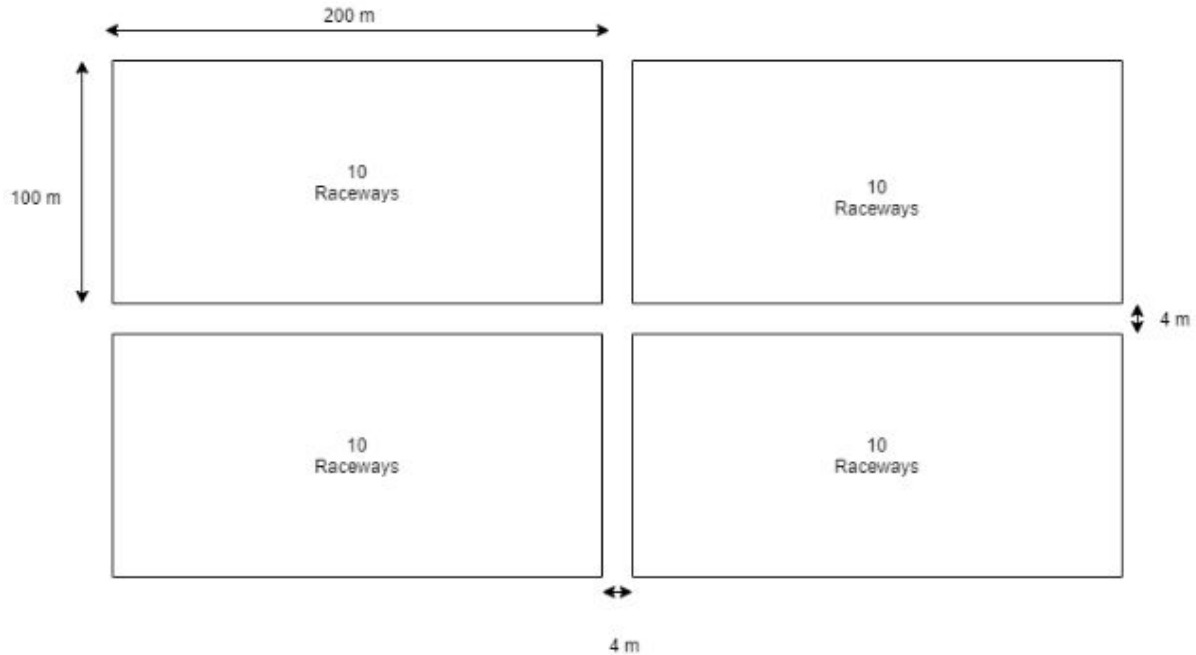


Figure 3-1-07: General raceway layout

Ten raceways will be laid next to each other, and these pockets of raceways will all be separated with a 4 meter walkway. This layout design was chosen in order to allow for access to all raceways from the short end, while minimizing the land required.

3.1.5 Algae Harvesting

The purpose of this step is to separate the algae from the incoming algal broth and concentrate it. The desired algal concentration is 20 g/L for the acid pretreatment step, and the algae from the raceways is coming in at 0.22 g/L. In this step, approximately 99% of the water will be removed. It is worth noting that 20 g/L, while requiring the removal of a lot of water, is still relatively dilute, with the solids content only being around 2%.

A variety of harvesting and drying methods are available for algae, though all of them have their own set of difficulties. Algae harvesting is often the most difficult and cost intensive step in the algal biofuel production process, primarily due to the high amounts of water present. A common harvesting step that was considered for harvesting is microflotation, where small air bubbles are pumped through the algae broth, and with the help of a flocculant, the algae sticks to these bubbles and is carried to the surface of the water. However, this method is energy intensive and is generally used in order to concentrate algae to 10% or greater amounts solid (Singh et al., 2011).

Sedimentation is often used as the first step in algae harvesting, in order to get rid of excess water and reduce the cost of microflotation. However, in this case as the final desired content of solids is only 2%, only sedimentation will be utilized. A flocculant will be utilized as sedimentation, on its own, is extremely slow (Singh et al., 2011)

3.1.6 Flocculation

This flocculant was chosen as the flocculant due to the high iron tolerance of yeast and the relative cost of the flocculant to other polymer based flocculants that tend to be non-toxic. The limit at which aluminum sulfate, a common flocculant, is toxic to yeast, is 2 mM, which is well below the final concentration of aluminum after sedimentation, of around 20 mM that will be required based off of preliminary calculations (Chatsungnoen & Chisti, 2016; Zheng et al., 2007).

In their study, Chatsungneon and Christi (2016) determined that 50 mg/L of FeCl_3 with a mixing time of 30 minutes and settling time of 30 minutes, resulted in a 95% yield of algae.

Mixing speed and time is important in flocculation as it impacts the final characteristics of the flocs formed.(Chatsungnoen & Chisti, 2016). Zhang et al. found that the shear rate of 9 s^{-1} was optimal in creating flocs that had the largest settling time (Zhang et al., 2019). At larger shear rates, flocs break apart due to turbulent mixing but at lower shear rates, the algae is not well mixed enough to form flocs. In order to achieve a high settling time, the flocs must be both large and compact (Zhang et al., 2019).

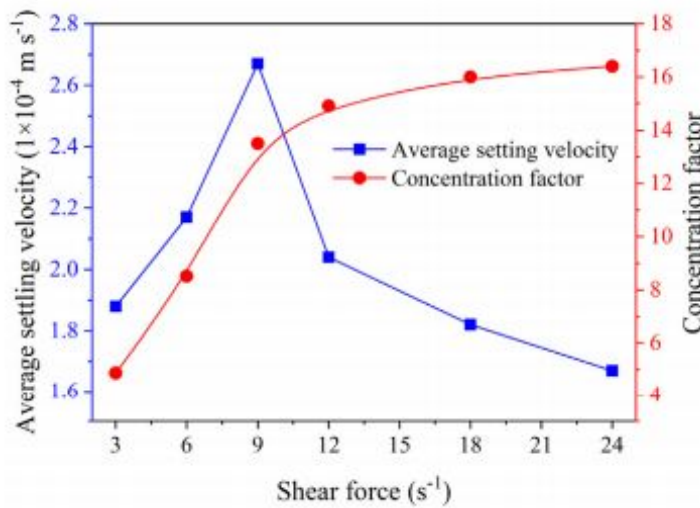


Figure 3-1-08: Average settling velocity and concentration factor vs. shear force (Zhang et al., 2019)

The mixing tanks were designed to operate at 9 s^{-1} shear rate. Shear rate is directly proportional to mixing rotation speed. An accepted constant of proportionality between shear rate and rotation speed, K_s , for a Rushton blade impeller is 11.5 (Wu et al., 2006). Using this constant, the appropriate mixing speed was determined to be 47 rpm to achieve the desired shear rate. It is worth noting in their study, Zhang et al. used Aluminum chloride as their flocculant and thus we are assuming that using another flocculant will not result in a different optimal shear rate. This assumption should be tested using our tank design specs and flocculant.

The mixing tank and impeller dimensions were determined using accepted typical tank dimension ratios (McCabe et al., 2005)

The Reynolds number of each tank was determined to be over 3000000, which suggests a turbulent regime. The power number was determined to be 6, and using the power number and the equation below, power consumption of mixing was determined.

$$P = N_p \rho n^3 D^5$$

The power required per mixing tank is 97 kW, with the total power needed to mix all 62 tanks is around 6000 kW.

3.1.7 Sedimentation

For the sedimentation process, settling time was increased from the 30 minutes reported to an hour and we are assuming that this change will increase the yield from 95 to 98% (Chatsungnoen & Chisti, 2016). This assumption and increased settling time should be tested in order to ensure that the yield does indeed increase to that extent. The 6 thickeners will be receiving the flocculated algae coming from the 62 mixing tanks. Flow rate from each mixer would be approximately 0.2 m³/s, small enough to allow for gravity filling of the settlers. This would allow for the algae flocs to maintain their shape and compactness, helping them settle.

Dimensions of the sedimentation tank were chosen in order to result in a residence time of approximately an hour. Approximately 1% of the incoming solution was designated to be removed as underflow, as the rest would leave the sedimentation tank as overflow. Stokes law was utilized to determine the terminal velocity of the algal flocs, utilizing the floc diameters reported (Zhang et al., 2019).

$$v = \frac{4gd^2(\rho_p - \rho_f)}{18\eta}$$

The settling velocity of the flocs is 3.5 mm/s and thus the flocs can settle down up to approximately 12 meters in an hour. This ensures that the flocs will have settled down over the 2 meter thickener height designated.

3.2 Algae Pretreatment

The unit operations downstream of algae harvesting were designed assuming the maximum recovery of 220 tons of algae per day. The 2% loss during sedimentation was not accounted for during design, however, and accordingly downstream mass flows and equipment are oversized by about 2%.

Park et al. (2015) reviews methods of lipid extraction from algae. Direct transesterification methods were not considered, since the cell mass is more difficult to track and is to be used for ethanol production. Hot water extraction was chosen due to the simple conditions not requiring specialized equipment, the lack of organic solvents needed, and relatively high yield. Additionally, the acidic conditions are sufficient to hydrolyse cellulose to glucose at the same time, reviewed below.

Microalgal carbohydrates are lignin-free which allows a simple conversion to sugars. Ho et al. (2013) found at 1% H_2SO_4 by volume, 20 g/L algae density, 120°C temperature, and 20 minute residence time, 97.6% of cell carbohydrates are converted to sugars, with 97.2% of the carbs becoming glucose. Park et al. (2014) found at the same conditions except for H_2SO_4 being 1% by weight, that 291 mg lipids/g cell of 391.6 mg lipids/g cell (or 76.3%) were able to be extracted. It is assumed that lipid conversion will be the same at the slightly higher 1% acid by volume, rather than weight. It is also assumed the same proportion of carbohydrates and lipids are converted as in these studies, although the absolute concentration of each component is different with the chosen strain of algae.

To estimate the viscosity of the mixture, the viscosity versus volume fraction of Adesanya et al. (2012) was used. The linear, intrinsic viscosity relationship at low concentrations based on their Fig. 4 was estimated to be:

$$\mu = \mu_{water} (1 + 16.9 * [volume\ fraction\ algae])$$

At the given concentrations, the viscosity is found to be marginally higher than water, with 0.30 mPa*s versus 0.23 mPa*s for the given conditions.

The acid-catalyzed decomposition of glucose can reduce the available glucose for fermentation and possibly be toxic to the yeast. Experimental kinetics for this reaction have only been performed above 100°C (Gurgel et al., 2012; Pilath et al., 2010). Extrapolating the kinetic expression found to 35°C shows the glucose decomposition to be negligible, thus the solution is cooled immediately after reacting to prevent decomposition. The reactor was chosen to be a plug flow reactor to control residence time, both to avoid decomposition and conform to the residence time of Park et al. (2014) and Ho et al. (2013). Since flow is turbulent and the length of the reactor is much longer than the diameter, ideal PFR behavior is assumed.

Cellulose hydrolysis is endothermic with a reaction energy of 21 kJ/kg cellulose (Kunihisa & Ogawa, 1985). At the concentration and extent of cellulose reacted, this results in a negligible temperature drop of 0.03°C. With forced convection in the pipes and natural convection outside the half-inch insulation, the heat loss to surroundings results is also negligible at a 0.02°C temperature drop.

3.3 Lipid Extraction

3.3.1 Lipid Separation with Hexane

After the lipids are released from the cells, a mixture of lipids, cell matter, glucose, proteins, sulfuric acid, and water remains. The lipids at this point are assumed to be triolein to ease calculations. Given its abundance and the similarities to other lipids present, this was deemed an appropriate assumption. This mixture is unusable as is, so certain components must be removed to allow for ethanol and biodiesel production. The lipids must be the first component removed. The pure lipids will be used for biodiesel production, while the remaining mixture will be further purified downstream to isolate the cell matter and produce ethanol.

The lipid in the mixture, triolein, is a type of triglyceride (LaMorte, 2016). Triglycerides have a 3 carbon “glycerol backbone” with a fatty acid coming off of each carbon. In the case of triolein, pictured in Figure 3-3-01, each of these fatty acid chains consist of 18 carbons with a double bond between the 9th and 10th carbons (PubChem, n.d.).

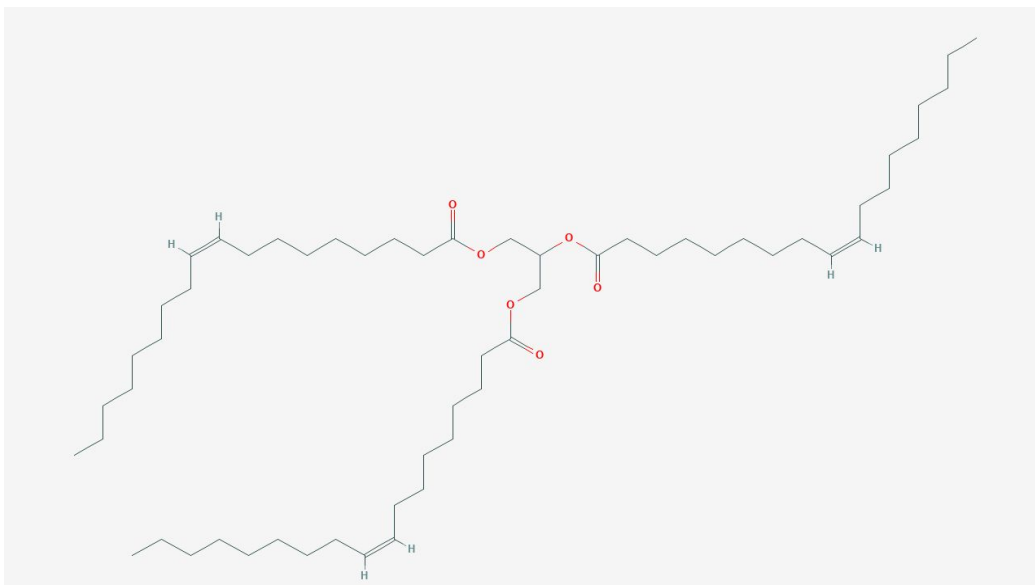


Figure 3-3-01: Triolein Molecule

The triolein can be separated using its nonpolar nature. This lack of polarity means that there is not a concentration of positive or negative charges in any one part of the molecule. Contrasting to water, which is extremely polar, the difference between the two forces the lipids to separate from the rest of the mixture and form a separate layer.

To ease the process of separating the lipids, a second nonpolar substance can be added to increase the size of the layer. In this case, hexane will be used. Since the hexane is also nonpolar, the lipids and the hexane will form a miscible layer separate from the rest of the mixture, allowing for liquid-liquid extraction. Liquid-liquid extraction utilizes the difference in polarity of the substances in the mixture to separate them from one another (*Liquid-Liquid Extraction*, 2013).

The separation will be done using a horizontal decanter and will allow for full recovery of the hexane and lipid layer (Park et al., 2014). In this decanter, the entire mixture will be allowed to settle and separate into 2 layers. The top, nonpolar layer consists of hexane and lipids, and the bottom, polar layer has water, sulfuric acid, cell matter, proteins, and carbohydrates. In this tank, a vertical wall with some space in between its top and the tank ceiling allows the top layer to pour over into the rest of the tank. The top layer pouring over creates the physical separation between the hexane and lipid layer from the rest of the mixture. The hexane and lipid layer is then sent down the biodiesel production line while the polar, cellulosic mixture is sent to the ethanol production line.

3.3.2 *Hexane Recovery*

Coming from the decanter, the hexane and lipids are in a homogenous mixture which must be separated. The hexane is valuable for recycling back to the decanter to minimize input costs, and the lipids need to be extremely pure in order for proper transesterification of biodiesel to occur. To do this, the mixture is put through a vacuum evaporator. The hexane evaporates very easily, with its nonpolar nature and small molecular mass. Contrarily, the lipid has a molecular mass ten times greater than the hexane, making it require more energy to vaporize. This difference in volatility, or the ease at which the component can vaporize, encourages the hexane to evaporate while the lipid stays in liquid form. By dropping the pressure in this vessel, the process is accelerated to allow the evaporator to maintain steady-state conditions.

3.4. Biodiesel Production and Purification

The purpose of this section of the design is to take the algal oil, separated from hexane in the extraction step, and convert it into fatty acid ethyl esters (FAEEs)/biodiesel using a transesterification reaction and purify it to at least 99.5% biodiesel by mass for sale as fuel using two distillation columns and a two-phase gravity settler with secondary flash.

The basic flow of the process, which will be broken down in detail subsequently, involves the joining of two recycle loops (unreacted ethanol and oil) with incoming ethanol and algae oil, the conversion of oil and ethanol to biodiesel and glycerol, distillation of unreacted ethanol, and purification of biodiesel using phase separation and distillation, with the unreacted oil being recycled. See Figure 4-4-01 in Section 4.4 for a look at the overall process flow diagram; equipment names in this section are referenced from there as well.

Calculations were performed in Aspen Plus, and algae oil was approximated as triolein as it's present in large quantities in algal oil. The UNIQUAC activity coefficient model and Redlich-Kwong equation of state were used for property calculations (Patle et al., 2015; Rostami et al., 2012). Binary interaction parameters were tabulated from Aspen databases for hexane/(ethanol, water) and ethanol/(water, glycerol) and water/glycerol. In order to attempt to properly account for liquid-liquid interactions between all components, the remaining missing binary interaction parameters were calculated using UNIFAC as there was no data available for these. It would be useful to collect this data experimentally if this design were to be carried out to ensure calculation accuracy.

Lastly, stage efficiencies for distillation columns were estimated from an empirical correlation relating efficiencies to average viscosity from Peters et al. (2003), Equation 15-35. This resulted in an estimated stage efficiency of about 0.55 for both columns T-401 and T-402.

3.4.1 Supercritical Transesterification of Algal Oil to Fatty Acid Ethyl Esters (FAEEs/Biodiesel)

The transesterification reaction converts oil (triglycerides) and ethanol into glycerol and biodiesel, and it takes place at the conditions for supercritical ethanol (Figure 3-4-01) in reactor R-401.

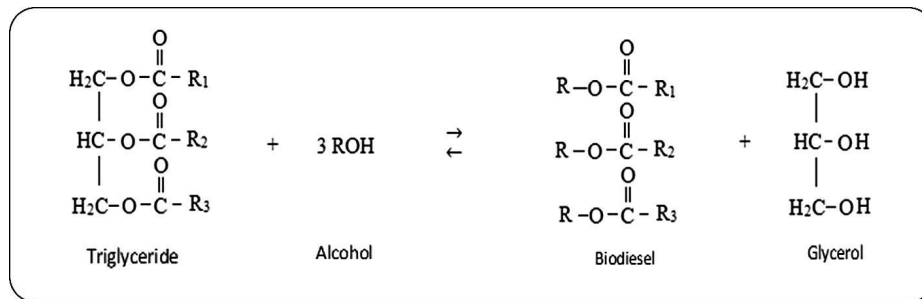


Figure 3-4-01: Transesterification reaction (Santana et al., 2016).

Supercritical transesterification is energy-intensive and requires high temperatures and pressures but simplifies separations considerably as it allows the reaction to occur without an acid or base catalyst. In a catalyzed transesterification, the catalyst would need to be removed and regenerated from the product. Additionally, catalyzed reactions have the potential to make undesirable waste products like soap in the case of an alkali-catalyzed reaction (Deshpande et al., 2017). Thus, the supercritical method was deemed to be superior for this application.

Additionally, since the high temperatures required of this reaction are not needed elsewhere in the process and since high pressure steam is not a preferable way to reach temperatures as high as what's required, there is a local furnace H-401 that heats a

high-temperature heat transfer oil in a closed loop (indicated by the dashed lines in the PFD Figure 4-4-01) which provides all of the heating for this process. Since the reactor is at a higher temperature than the rest of the process, it's possible to run the heat transfer oil in series through each of the heat exchangers adding heat to a process fluid.

Since real algal oil is composed of several different types of fatty acids and exact lipid profiles can vary based on species and growth conditions (Yaşar & Altun, 2018), a kinetic evaluation of reaction rate and conversion would be difficult, given that each different fatty acid would require its own rate expression. Moreover, kinetics of individual lipids in this reaction are not readily found in literature. Therefore, a decision was made to use an empirical yield correlation to calculate conversion.

The yield correlation was taken from Nan et al. (2015) and is a function of temperature, pressure, alcohol-to-oil molar ratio, residence time, and alcohol water content mass %; the R^2 value for the correlation is 0.9718, indicating that it should be fairly reliable, at least for first-order calculations. An important caveat is that the correlation was calculated for *Chlorella protothecoides* rather than *Chlorella vulgaris* as we are using. It would be prudent to run similar experiments with *Chlorella vulgaris* to ensure that the results hold or otherwise need to be adjusted. Since the two species are within the same genus, there should be some similarity in the results, however, increasing confidence in the results.

The reactants are brought up to supercritical conditions by first pressurizing the two liquid streams (oil and ethanol/water) to 170 bar at normal temperatures to avoid the high costs of compressing gases to such a pressure and then heating them both to 340°C. The reaction is performed isothermally to provide a consistent result from the yield correlation and to prevent

the reaction from going beyond the temperature limits of the correlation as 340°C is already near the upper temperature limit tested by the authors, and it's preferable to avoid extrapolation.

However, the reaction is just slightly exothermic, so little cooling is required.

The reaction is run at a 33:1 alcohol-to-oil molar ratio, which amounts to about a 1.75:1 ratio by mass. Because this reaction is run in such a large excess of ethanol, an ethanol recycle stream is required, and relatively smaller amounts of makeup ethanol are required to continue running the reaction.

3.4.2 Product Separation and Purification of Biodiesel

The stream leaving the reactor R-401 contains unreacted ethanol and oil, biodiesel from the recycle stream, glycerol, and water. Separations can be split broadly into 1) removing ethanol and water to be recycled and run through the reactor again and 2) purifying the biodiesel through the removal of glycerol, unreacted oil, and remaining ethanol and water. The first separation takes advantage of the immense difference in volatility between ethanol/water and biodiesel, glycerol, and oil, and the second set of separations primarily takes advantage of the development of multiple phases between glycerol and biodiesel/oil but also of the volatility difference between biodiesel and unreacted algal oil.

The products leaving the reactor are first depressurized in an adiabatic expansion down to 7 bar before entering the ethanol distillation column T-401. This will lower the cost of the column since it will not have to accommodate as extreme pressures as found in the reactor. Additionally, the drop from 7 bar to atmospheric pressure later on in the secondary flash S-402

after phase separation in the settler S-401 is sufficient to remove remaining impurities in the biodiesel to allow a sale-purity product after distillation.

So, the distillate of the ethanol distillation column T-401 consists of almost completely ethanol and water, with negligible quantities of remaining components, and the bottoms contains mostly biodiesel with smaller quantities of unreacted oil, glycerol, ethanol, and water. The distillate is decompressed and condensed for mixing with the makeup ethanol/water mixture (needs to be condensed as the stream must be completely liquid going into the pump), and then the combined stream is pumped back to 170 bar and heated to 340°C for the reaction again. The bottoms is sent to the gravity settler S-401 to further purify the biodiesel.

In the gravity settler S-401, over the course of 4-8 hours (Clifford, n.d.), the liquid will separate into a polar phase consisting of primarily glycerol with minor amounts of ethanol and water and a nonpolar phase consisting mostly of biodiesel and unreacted oil. The glycerol phase can be drawn off to be handled as waste, and due to the lack of catalytic elements in this process, is pure enough to not require significant additional handling (96.4% glycerol, 2.8% ethanol, 0.6% water, 0.2% other) and even could likely go through minor treatment to reach sale quality. The biodiesel phase is sent through a secondary flash S-402 down to atmospheric pressure to remove additional ethanol, water, and glycerol from the biodiesel phase (though some biodiesel is removed as well), and then to the biodiesel distillation column T-402 for final purification.

In the biodiesel distillation column T-402, the primary separation is between unreacted oil and biodiesel. The column is run at significant vacuum pressure (0.05 bar) in order to reduce the temperature of the reboiler down to about 333°C; the reboiler temperature at normal pressure is around 600°C. This is necessary as biodiesel and oil have an increased likelihood of

decomposition at such high temperatures, which would reduce product purity and introduce components which were unaccounted for in this design. The distillate stream is the biodiesel product, purified to specifications for sale (99.7% pure), and the bottoms stream is recycled into the oil stream from lipid extraction.

3.5 Fermentation Pretreatment

3.5.1 Neutralization

The purpose of neutralization is to bring the glucose solution to conditions acceptable for yeast fermentation. For this purpose, the neutralization must both bring pH and ion concentrations to acceptable levels. To perform the mass and energy balances, an Aspen Plus mixing block was used with the electrolytes package.

The reactor was chosen to be a continuous stirred tank reactor (CSTR) to allow input of the solid calcium hydroxide and allow residence time for gypsum (calcium sulfate dihydrate) to crystallize. The mixing is performed at 0.09 kW/m^3 , close to Peters et al.'s (2003) heuristic for blending (0.1 kW/m^3). The time needed to dissolve the calcium hydroxide is neglected. The tank material is 316 stainless steel to prevent corrosion from any residual sulfuric acid, as well as ferric chloride, during neutralization.

Multiple bases were considered for neutralization. Sodium hydroxide would produce sodium sulfate salt, which is highly soluble in water leaving high concentrations of sodium and sulfate ions which is unacceptable to yeast. Barium hydroxide would produce insoluble barium sulfate which can be nearly completely removed, however the cost per hydroxide ion is nearly ten times that of calcium hydroxide.

Calcium hydroxide produces calcium sulfate which is partially soluble, precipitating gypsum (calcium sulfate dihydrate) with 2.01 g/L remaining in solution. The calcium ion inhibits yeast growth and fermentation more than the sulfate ion (Maiorella et al., 1984). Some studies have shown this concentration of calcium ions to be inhibitory to growth and fermentations, while others place it well below inhibitory concentration (Maiorella et al., 1984; Richards, 1925).

It is assumed in design that this level is non-inhibitory. If calcium ions would need to be further removed, a second reaction could precipitate insoluble calcium carbonate or calcium oxalate, replacing calcium with a less inhibitory cation.

The neutralization reaction precipitates gypsum crystals. The rate of calcium sulfate crystallization and size distribution of gypsum crystals depends on the level of supersaturation and impurities present (Budz et al., 2007; McCall & Tadros, 1980). Smith & Sweett (1971) found at levels of supersaturation up to 1.81, crystallization is almost complete after 20 minutes. Since the level of supersaturation at mixing is at 13.4, it is assumed 5 minute resident time is sufficient. While CSTR assumptions would require a supersaturation driving force at outlet conditions, this is neglected since the evaporator will further increase supersaturation shortly. An accurate assessment of crystallization rate and size in the process conditions would require direct study. Crystal size is further discussed in Section 3.5.3.

3.5.2 Evaporation

The purpose of this step is to concentrate the glucose solution to levels standard for yeast fermentation.

To model the process, an Aspen Plus Flash2 block was used with the electrolytes package. The fraction of inlet vaporized was adjusted, in conjunction with filtering, such that the filtrate flow out was 1500 m³/day. The model did not include components for remaining algae waste, so they were treated as part of the water stream. The true volume may be slightly lower due to higher density.

The input solution contains 2.8 wt% solids, which increases to 21 wt% primarily from removal of water but also further solid crystallization. To handle this process, crystallizers were rejected as the inlet already contains 93% of the solids that will be formed, and they focus on obtaining uniform, pure crystals as a product rather than just removal. To handle the slurry, agitated or scraped film evaporators were considered, but rejected due to low area of heat transfer per evaporator and high cost. Forced-convection evaporators had a similar cost, although a higher area. A natural convection, vertical long tube evaporator was used for high area and low cost. Since calcium sulfate scales surfaces and the long tube evaporator may not be able to handle the concentration of slurry, six evaporators were designed rather than the three needed for operation to account for maintenance. Scale model testing should be performed to determine if a forced convection evaporator would be required for operation.

At high temperatures, the thermodynamically stable solid phase of CaSO_4 is either solid CaSO_4 or $\text{CaSO}_4 \cdot \frac{1}{2} \text{H}_2\text{O}$, rather than $\text{CaSO}_4 \cdot 2\text{H}_2\text{O}$ (gypsum). However, the transformation between phases has been observed as kinetically slow (Nancollas et al., 1973). Since the residence time in the evaporator is relatively short, and the product is cooled afterward, non-gypsum solid phases are neglected. However, this may affect the crystal sizes and water balance in reality.

In thermal design, a preheating heat exchanger to bring the slurry near boiling was included such that sensible heat is ignored in the evaporator. The evaporators were designed as single-effect, but the economic tradeoff to be multiple-effect is discussed in Section 5.3.3. The overall heat transfer coefficient was estimated to be $2250 \text{ W/m}^2\text{K}$, based on nucleate boiling and film condensation on carbon steel tubes.

3.5.3 Rotary Vacuum Drum Filtration

Multiple choices are available to remove the gypsum crystals. Centrifugation is energy intensive, and washing would be required to recover entrained glucose from the solid crystals. Sedimentation was not considered due to the difficulty of estimating settling at high densities, and the large area needed. Membrane or crossflow systems are likely to gel, or get clogged, at the high density of solids present. Of cake filtration methods, rotary vacuum drum filtration was chosen as it is continuous and commonly used.

The drums were designed according to Eq. 30.29 of McCabe et al. (2005). Assumptions were made about the crystal sizes and properties of the solids cake. The crystals were assumed to uniformly be cylinders of 10 μm diameter and 100 μm length, as a lower range of crystals seen in research (Gominšek et al., 2005; Nancollas et al., 1973) since the crystallization had been at uncontrolled supersaturations and low overall residence times. The cake was assumed to be incompressible and 50% liquid by mass. Air was assumed to have 60% of the cake resistance as the filtrate, based on Peters et al. (2003) Ch. 15, to estimate the air intake of the vacuum pump. For the purposes of this design, the details of the vacuum system that separates air from the filtrate are not specified.

The properties of the feed and filtrate were estimated based on the algae waste and solids concentration. Algae waste assumed to behave as full-celled algae for the purposes of calculating the viscosity (Adesanya et al., 2012). The effect of the glucose on density and viscosity has been found to be negligible at this concentration (Comesaña et al., 2003).

Based on Ch. 30 of (McCabe et al., 2005), it was assumed a 1.5 ratio by mass of washing water for entrained liquid would recover 93% of the glucose solution.

3.6 Fermentation and Ethanol Purification

The purpose of the fermentation is to convert the sugars made during pretreatment and convert it to dilute ethanol using yeast (*saccharomyces cerevisiae*). The dilute ethanol is then brought to a fuel grade concentration of 99.5% (U.S. Department of Energy, 2018) with a series of separators; the concentration is achieved by centrifugal solids separation followed by distillation then zeolite azeotrope breaking.

3.6.1 Continuous Fermentation

Continuous fermentation is designed to take the glucose sugar stream concentrated during fermentation pretreatment (stream 509) and convert as much as possible into ethanol using *saccharomyces cerevisiae*. There were two primary decisions made on how to most logically convert sugars to ethanol: the fermenting microbe and the method of fermentation.

The fermenting microbe could have been a bacterial strain, genetically modified yeast for optimized conversion rates, or standard brewer's yeast. Bacterial fermentation microbes had far less available rate data, which would make running simulations difficult and increase the number of assumptions made. Additionally, they are harder to clean out of the equipment due to their size and flocculation tendencies. A genetically modified yeast strain could increase the rate of production, but these are significantly more expensive than commercially available counterparts. *Saccharomyces cerevisiae* (brewer's yeast) is a cheap, available, and resilient strain of microbe capable of converting to the product in the desired time frame. It also has ample available rate data so few assumptions need to be made about the conversion. For these reasons it was chosen as the microbe for fermentation.

The method of fermentation was a choice between either batch fermentation or continuous operation. Batch reactors would need to be large and plenty enough to convert the volume of liquid being processed (1500 m³/day). Continuous operation allowed the total volume of the reactors (900 m³) to be less than the total, which would save money on equipment. Batch reactors would also need to be inoculated and cleaned after each use. This would make for both increased costs in yeast purchasing or recovering and operation/labor. By using continuous operation, the vessels washout the yeast as it is being made, so no additional yeast needs to be added other than getting the CSTR's to a continuous state. The process flow was modeled after Vogelbusch MultiCont continuous alcohol fermentation system (Vogelbusch, 2018).

This process is done via a type I fermentation where yeast break glucose into ethanol and release carbon dioxide. The fermentation is a fairly simple reaction whose kinetics can be modeled using the concentrations of the constituents. To model the kinetics of the reaction the Monod equations were used. This model is widely used in biology and biochemistry in order to accurately predict substrate concentration, cell mass, and product concentration. The parameters for the monod equations were taken from a study done on yeast with different carbon sources (Krishnan et al., 1999). By the end of the fermentation the existing solution has an ethanol content of 3.2% by volume.

3.6.2 Solids Separation

The purpose of solids separation is to isolate the ethanol and water solution for further refinement. This is done by removing a solids slurry from the solution exiting the fermenter. There are many methods for separating entrained solids including but not limited to vacuum

drying, filtration, and centrifugation. Centrifugation was chosen above the others because a model cellulosic ethanol plant with comparable volumetric flow rates and stream composition recommended it for separation (McAloon et al., 2000). The recommendation stemmed from the economic benefit; there is minimal maintenance and operational cost compared to the other options. The centrifuge is able to continuously remove a solids slurry from the ethanol and cell matter solution exiting the fermenter. For the remaining downstream ethanol calculations, it was assumed that no solid matter affects the water ethanol interactions. This is then fed to the preliminary distillation which brings ethanol to a higher concentration.

3.6.3 Distillation to Azeotrope

Distilling to the azeotrope brings the ethanol solution as close to fuel grade specifications as possible. Since the solution coming into the distillation column has a low ethanol volume percent (~3), there is much more volume of bottoms waste water compared to ethanol distillate. For this reason, the separation is also used to drastically reduce the volume of the processed product stream. There were not many decisions to be made in terms of how the separation would operate. Various literature and research documents gave the column specifications: 20 stages minimum hence the 30 used with an assumed 70 percent stage efficiency (Katzen et al., n.d.); tray spacings of ~0.5 m (Katzen et al., n.d.) meaning a total height of 15 m; pressures operating at 1.8 bar (E. Anderson, February 2020).

The distillation was modeled in ASPEN Plus v11 using the RadFrac column and the SRK package. The reflux ratio was determined by using design specifications of product purity at 95.5% and a mole recovery of nearly 100% of ethanol in the distillate. The condenser leaves the

distillate as a vapor, as the next rectification stage requires the ethanol to be in a vapor phase. A feed bottoms exchanger is being used in this distillation in order to improve the heat recovery.

3.6.4 Azeotrope Breaking

Azeotrope breaking is the final step to get the ethanol solution to its required concentration of 99.5%. There were a couple of methods considered for accomplishing this separation: an added entrainer, or a zeolite column. An entrainer would require another recovery step in order to recharge the solution. This would mean more equipment and likely more costs to replace lost entrainer. Zeolite columns do not require extra recovery equipment but do need two columns, so that one can be recharged while the other is operating. Zeolites do not require purchases beyond the initial cost to pack the column. In a comparative study, it was found that zeolites/adsorption are innovative and can result in the highest ethanol purities (Zentou et al., 2019). For these reasons an aluminosilicate zeolite is being used for water adsorption in the final rectifying column.

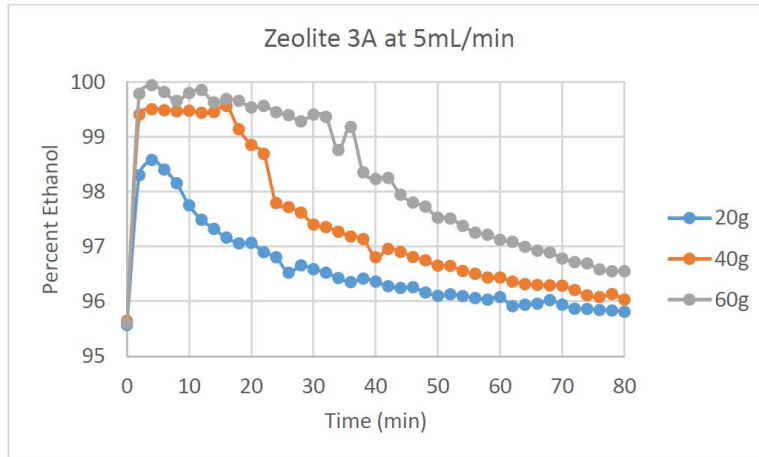


Figure 3-6-01: Comparing various masses of Aluminosilicate zeolite and product ethanol conc.

This experiment was at a lab scale and was used to scale the separator (Alameda et al., 2015)

The figure shown above and its corresponding research were used to estimate the dimensions and flow rates required for the final ethanol rectification. By scaling up the lab experiment, we were able to size an adsorption column which would rectify the ethanol to the required concentration. The residence time in the column does not exceed the 30 minute maximum shown in Figure 3-6-01.

4. Recommended Design

4.1 Algae Cultivation and Harvesting

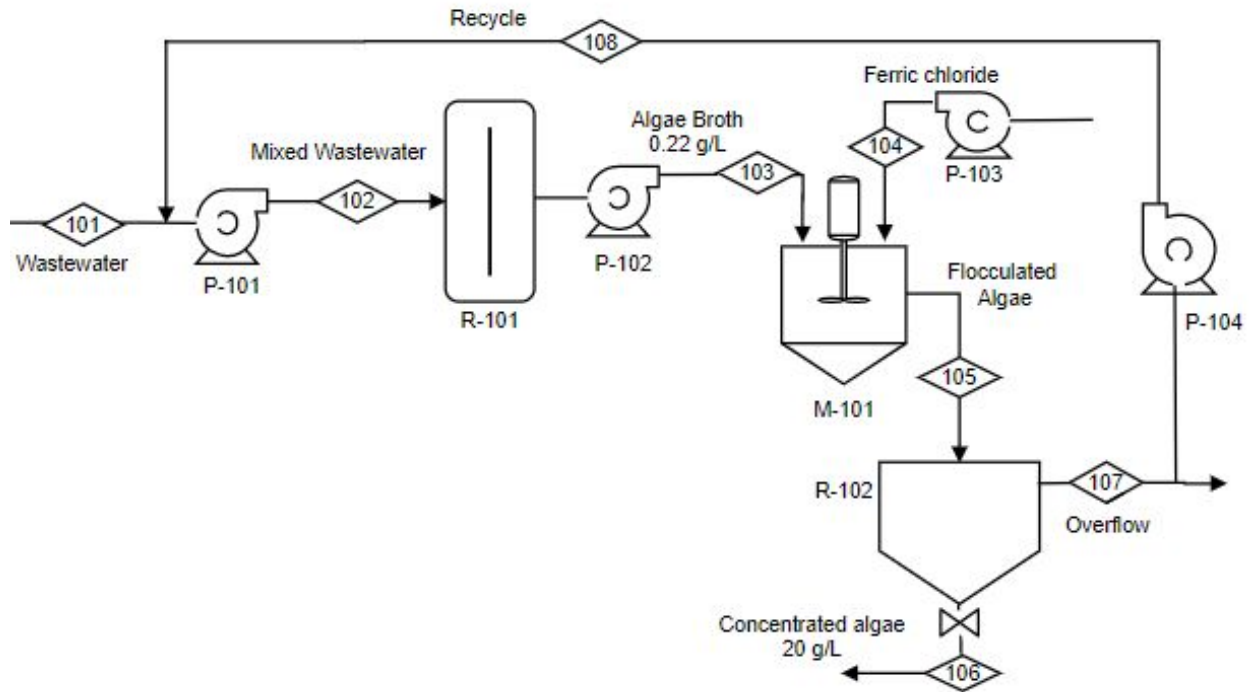


Figure 4-1-01: Algae Cultivation and Harvesting Process Flow Diagram

4.1.1 Algae Cultivation

Secondary wastewater (Stream 101) and recycled water (Stream 108) will be mixed (Stream 102) and fed by Wastewater Pumps, P-101, into one of seven designated Open Pond Raceway, R-101, batches. Each batch consists of 1451 open pond raceways, with a total of 10,157 raceways for the 7 weekly batches. In R-101, the algae will be allowed to grow and cultivated for 7 days. On the seventh day, algae will be pumped out of the Raceways, R-101, by the Algae Broth Pump, P-102, into the processing units. All pumps in this section are centrifugal pumps.

Table 4-1-01: Raceway R-101 Specifications

Total Raceways	9,142	Paddlewheel blades	8
Length (m)	100	Linear velocity (m/s)	0.2
Width (m)	10	Power consumption/unit (W)	195
Depth (m)	0.4	Total power (kW)	1,532

Table 4-1-02: Algae Cultivation Pump Specifications

Equipment	Name	Flow rate (m ³ /s)	Operating Quantity	Delta Pressure (bar)	Shaft Work (kW/pump)
P-101	Wastewater Pump	0.926	25	4	529
P-102	Algae Broth Pump	0.463	50	5	331

4.1.2 Algae Harvesting

The Algae Broth Pump, P-102, then pumps the algae broth, Stream 103, into the Mixing Tanks, M-101. The Ferric Chloride Pump, P-103, then pumps 125,000 kg/day of ferric chloride solution into Mixing Tanks, M-101. The ferric chloride is allowed to mix with the algae broth in M-101 for 15 minutes to form algae flocs.

Table 4-1-03: Mixer M-101 Specifications

Total Mixers	62	Type of impeller	Rushton
Residence time (mins)	15	Number of blades	6
Tank diameter (m)	6	Impeller diameter (m)	2
Tank height (m)	6	Baffle width (m)	0.5
Power consumption/unit (kW)	97	Impeller height from bottom (m)	2
Total power (kW)	6,008	Width of impeller blade (m)	0.4
		Height of impeller blade (m)	0.5

After the formation of algae flocs, the algae is allowed to flow into the Sedimentation Tanks, R-102, via gravity. The residence time for the algae in R-102 is an hour. An underflow of concentrated algae, Stream 106 leaves the settlers. Stream 107 overflows out of R-102 as more algae is fed into the settlers. Approximately 5% of this stream is recycled into the incoming wastewater using the Recycle Pump, P-104. The remaining content of Stream 107 is sent back to the wastewater facility.

Table 4-1-04: Sedimentation Tank R-102 Specifications

Total Thickeners	6	Feed flow rate (m ³ /s)	1.93
Residence time (hour)	1	Underflow rate (m ³ /s)	0.02
Diameter (m)	70	Overflow rate (m ³ /s)	1.91
Height (m)	2	Volume capacity (m ³)	14,500

Table 4-1-05: Algae Harvesting Pump Specifications

Equipment	Name	Flow rate (m ³ /s)	Operating Quantity	Delta Pressure (bar)	Shaft Work (kW)
P-103	Ferric Chloride Pump	0.001	1	1	0.146
P-104	Recycle Pump	0.620	1	4	354

Below is a table summarizing the composition of each stream.

Table 4-1-06: Algae Cultivation and Harvesting Balances

Stream Number	101	102	103	104	105	106	107	108
Water (m ³ /day)	946,360	1000000	1000000	75	1000075	10,790	989,290	53,640
Algae (kg/day)	0	236	220,000	0	220,000	215,600	4,400	236
Carbs (kg/day)	0	80	74,800	0	74,800	73,304	1,496	80
Lipids (kg/day)	0	70	66,000	0	66,000	64,680	1,320	70
Proteins (kg/day)	0	85	79,200	0	79,200	77,616	1,584	85
Ferric Chloride (kg/day)	0	1,377	1,377	50,000	51,350	25,675	25,675	1,377

4.2 Algae Pretreatment

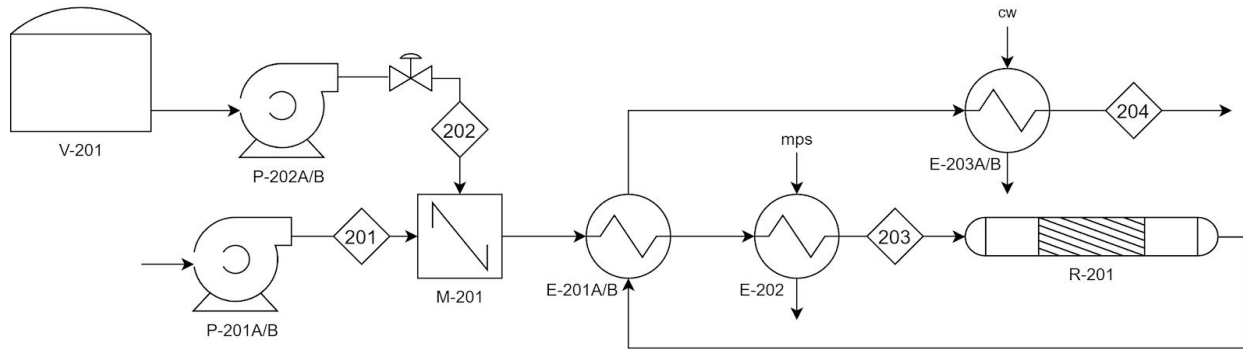


Figure 4-2-01: Algae Pretreatment Process Flow Diagram

Algae Pump P-201 brings the algae mixture Stream 106 to 4 barg, driving it through the Acid-Algae Mixer M-201, Plug Flow Reactor R-201, and Heat Exchangers E-201, E-202, and E-203. The high pressure stops the mixture from vaporizing at 120°C. The pump is stainless steel to resist ferric chloride corrosion. Acid Pump P-202 injects sulfuric acid from the 3600 m³ Acid Tank V-201 into the Acid-Algae Mixer M-201 at 4.5 barg. The Acid-Algae Mixer M-201 is a standard, grade 316 stainless steel pipe tee, allowing mixing in the turbulent conditions. The Feed-Effluent Heat Exchanger E-201A/B heats the feed acid-algae mixture from 30°C to 100°C, while simultaneously cooling the reactor effluent from 120°C to 50°C. The acid-algae mixture is fully heated to the reaction temperature of 120°C by Feed Heater E-202 with medium pressure steam. This heater is large enough to fully heat the feed during start-up. The grade 316 stainless steel Plug Flow Reactor R-201 has a residence time of 20 minutes, converting algal cellulose to glucose and freeing lipids for extraction. The reactor is covered by half an inch of insulation for safety. After the effluent is brought to 50°C by the Feed-Effluent Heat Exchanger E-201A/B, Effluent Cooler E-203A/B further quenches the mixture to 35°C to prevent side reactions.

Table 4-2-01: Algae Pretreatment Mass Flows; Ferric Chloride Omitted

Stream Number	201	202	203	204
Temperature (°C)	30	30	120	35
Pressure (barg)	4	4.5	2.5	1.5
Water (kg/day)	10,762,700	0	10,762,700	10,754,600
H ₂ SO ₄ (kg/day)	0	199,000	199,000	199,000
Carbs (kg/day)	74,800	0	74,800	1,800
Sugars (kg/day)	0	0	0	73,000
Glucose (kg/day)	0	0	0	72,700
Lipids (kg/day)	66,000	0	66,000	66,000
Extractable (kg/day)	0	0	0	50,300
Proteins (kg/day)	79,200	0	79,200	79,200

Table 4-2-02: Algae Pretreatment Equipment Specifications; Note: Fl.H.- Floating Head, 316SS- grade 316 stainless steel, CS - carbon steel; Areas are per heat exchanger, not total; temperatures are maximum expected

Heat Exchangers	E-201A/B (2 operating)	E-202	E-203A/B (2 operating)	
Type	Fl.H.	Fl.H.	Fl.H.	Fl.H.
Area (m ²)	1036	249	701	
Heat Duty (MW)	35.2	10.8	-10.8	
Shell				
Temp (°C)	120	184	45	
Pressure (barg)	2.5	10	0.5	
MOC	316SS	CS	CS	
Tube				
Temp (°C)	100	120	50	
Pressure (barg)	4.0	3.5	2.0	
MOC	316SS	316SS	316SS	
Reactor	R-201	Pumps	P-201A/B	P-202A/B
Temp (°C)	120	Type	Centrifugal	Centrifugal
Pressure (barg)	3.0	Flow (kg/s)	127.0	2.303
Length (m)	790	Fluid Density (kg/m ³)	1005	1830
Diameter (m)	0.5	Shaft Power (kW)	72.3	0.809
MOC	316SS	Efficiency (%)	70	70
		Pressure in (barg)	0	0
		Pressure out (barg)	4	4.5
		Temp (°C)	30	30
		MOC	316SS	316SS

4.3 Lipid Extraction

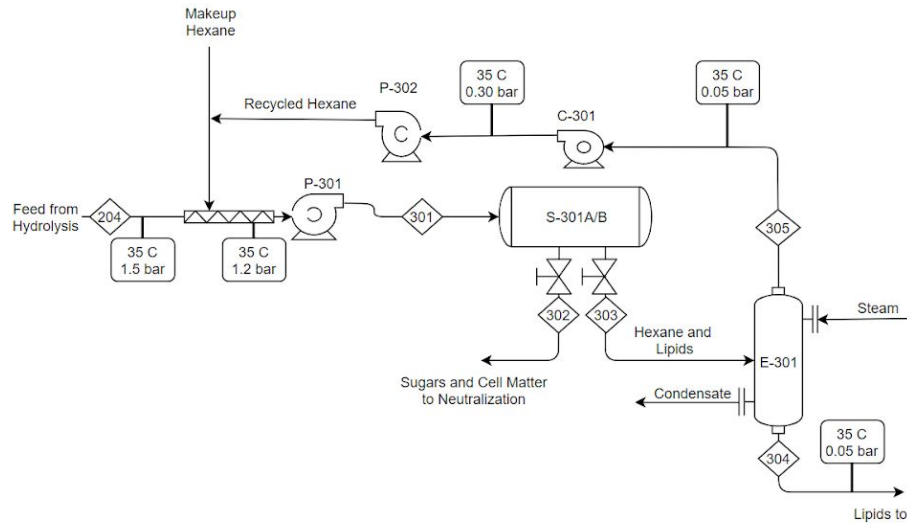


Figure 4-3-01: Lipid Separation and Hexane Recovery Process Flow Diagram

4.3.1 Lipid Separation with Hexane

The feed from the algae hydrolysis, stream 204, is mixed incoming hexane with an in-line static mixer to ensure full homogeneity of the mixture. In the static mixer, walls at different points within the tube create turbulence and fully mix the components. The incoming feed is at 35 °C and at startup is mixed with room temperature makeup hexane, so no cooling apparatuses are necessary. The hexane is mixed with the feed using a static, in-line mixer to ensure a homogeneous mixture before reaching the liquid-liquid extraction step. This method of mixing creates a small pressure drop, which pump P-301 resolves. This mixture is then sent from P-301 to horizontal decanters S-301A/B to separate the lipid and hexane layer from the rest of the mixture. S-301A/B are made of grade 316 stainless steel and each have a residence time of 30 minutes.

Upon separation, the sugars, cell matter, protein, carbohydrates, and sulfuric acid move to the neutralization process. The lipid and hexane layer is moved to vacuum evaporator S-302. Coming from S-301A/B, no temperature or pressure change occurs or is induced, for separation occurs solely because of the difference of polarities of the components.

4.3.2 Hexane Recovery

Vacuum evaporator E-301 drops the pressure of the lipid and hexane mixture from 1.5 bar to 0.05 bar, therefore forcing the hexane to vaporize. The gaseous hexane is separable from the remaining liquid lipids. 358.491 kW of energy is released due to the heat of vaporization of the hexane, so the separator is encased in a slightly larger vessel where low pressure steam (4 barg) is piped into the shell side. E-301 is made of 316 stainless steel. Once the lipids and hexane are separated, the lipids move to the transesterification process while the hexane is recycled back to be mixed with the feedstock.

Before being remixed with the feedstock, the hexane must be condensed into liquid. Compressor C-301 compresses the gaseous hexane isothermally to condense it and bring it to the liquid form. This condensation is necessary to properly mix the hexane with the feedstock. From condensing, pump P-302 further raises the pressure of the liquid hexane to combine it with the makeup hexane and later mix it with stream 204.

In order to keep the hexane in the system at 1,000,000 kg/day, there is a makeup hexane requirement of 34 kg/day.

Table 4-3-01: Mass Balance around S-301A/B

Stream	301	302	303
Temperature (°C)	35	35	35
Pressure (bar)	1.5	1.5	1.5
H ₂ O (kg/day)	10,754,600	10,754,600	0
H ₂ SO ₄ (kg/day)	199,000	199,000	0
Carbs (kg/day)	1,800	1,800	0
Sugars (kg/day)	73,000	73,000	0
Lipids (kg/day)	50,300	0	50,300
Proteins (kg/day)	79,200	79,200	0
Hexane (kg/day)	1,000,000	00	1,000,000

Table 4-3-02: Mass Balance Around E-301

Stream	303	304	305
Temperature (°C)	35	35	35
Pressure (bar)	1.5	0.05	0.05
Lipids (kg/day)	50,330	50,330	~0
Hexane (kg/day)	1,000,000	34	999,966

Table 4-3-03: Lipid Extraction and Algae Recovery Equipment Specifications. All specifications are per piece of equipment, not total requirement.

Heat Exchangers	E-301
Type	Shell and Tube
Area (m ²)	94.25
Heat Duty (kW)	358.5
Shell	
Temperature (°C)	35
Pressure (bar)	0.05
MOC	316SS
Tube	
Temperature (°C)	142
Pressure (bar)	4
MOC	316SS
Separators	S-301A/B
Temperature (°C)	35
Pressure (bar)	1.5
Length (m)	10
Diameter (m)	6
Duty (kW)	0
MOC	316SS
Compressor	C-301
Type	Centrifugal
Volumetric Flow (m ³ /s)	0.017536
Pressure in (bar)	0.05
Pressure out (bar)	0.30
Differential Pressure (Pa)	126,325
Power (kW)	2.215
MOC	316SS

Pumps	P-301	P-302
Type	Centrifugal	Centrifugal
Volumetric Flow (m ³ /s)	0.142778	0.017536
Pressure in (bar)	1	0.30
Pressure out (bar)	1.5	1.5
Differential Pressure (Pa)	50,662	222,915
Power (kW)	7.233	3.909
MOC	316SS	316SS

4.4 Biodiesel Production and Purification

The overall process flow diagram for biodiesel production and purification is shown in Figure 4-4-01. The main points of interest are the reactor R-401, two distillation columns T-401 and T-402, and two-phase gravity settler S-401 with secondary flash S-402. These pieces of equipment and the surrounding streams and ancillary equipment will be discussed in Sections 4.4.1, 4.4.2, 4.4.3, and 4.4.4.

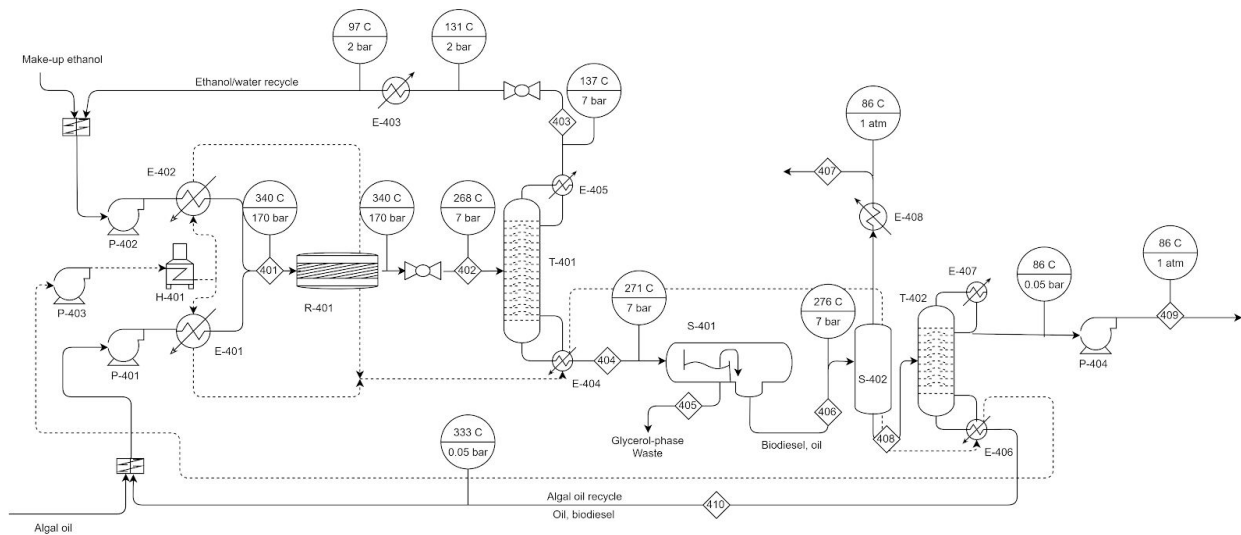


Figure 4-4-01: Biodiesel Production and Purification Process Flow Diagram. Dashed lines indicate heat transfer oil flow path from heater.

4.4.1 Transesterification Reactor

Algae oil from lipid extraction is combined with the oil recycle stream coming from distillation column T-402. Incoming makeup ethanol (~99.5% pure, as from purified fermentation ethanol) is combined with the ethanol/water recycle stream coming from the first distillation column T-401. The oil stream is compressed to 170 bar by pump P-401, and the ethanol stream is compressed to 170 bar by pump P-402. These are both run through heat

exchangers E-401 and E-402 to reach 340°C. The resultant mixed Stream 401 is sent to the reactor R-401, which performs the reaction isothermally; the products go through an adiabatic expansion to reduce pressure down to 7 bar, represented as Stream 402. The stream table is shown in Table 4-4-01, and reactor specifications are shown in Table 4-4-02.

Table 4-4-01: Transesterification Reactor R-401 Mass Flows

Stream Number	401	402
Temperature (°C)	340	268
Pressure (bar)	170	7
Ethanol (kg/day)	78100	70300
Water (kg/day)	8300	8300
Glycerol (kg/day)	0	5200
Biodiesel (kg/day)	200	53100
Algal Oil (kg/day)	55200	4900

Table 4-4-02: Transesterification Reactor R-401 Specifications

Diameter (m)	2
Length (m)	4
MOC	316SS
Residence time (min)	35

4.4.2 Ethanol Separation and Recycle

The low-pressure transesterification products in Stream 402 go into distillation column T-401. Ethanol and water make up the bulk of the distillate in Stream 403, the ethanol recycle stream. Biodiesel, glycerol, and unreacted oil are the main components of the bottoms in Stream 404. Stream tables for this column are shown in Table 4-4-03, and column specifications are

shown in Table 4-4-04. The condenser and reboiler specifications are shown in Table 4-4-05.

Additionally, T-401 has a reflux pump P-405 whose specifications are found in Section 4.4.4.

Table 4-4-03: Ethanol Separation Column T-401 Mass Flows

Stream Number	402	403	404
Temperature (°C)	268	137	271
Pressure (bar)	7	7	7
Ethanol (kg/day)	70300	69500	800
Water (kg/day)	8300	8250	50
Glycerol (kg/day)	5200	0	5200
Biodiesel (kg/day)	53100	0	53100
Algal Oil (kg/day)	4900	0	4900

Table 4-4-04: Ethanol Separation Column T-401 Specifications

Stages	26 (24 trayed stages)	Height (m)	14.5
Condenser	Partial-vapor	Diameter (m)	0.6
Reflux Ratio	1	MOC	316SS
Feed Stage	9	Tray efficiency	0.55

Table 4-4-05: Ethanol Separation Column Condenser E-403 and Reboiler E-404

	Condenser E-403	Reboiler E-404
Duty (kW)	-800	490
Area (m ²)	8.6	9.8

4.4.3 Biodiesel Purification

The bottoms product from ethanol separation column T-401 goes into a two-phase gravity settler S-401 at atmospheric pressure; it remains there for an estimated 6 hours residence time on average to reach phase equilibrium. Two liquid streams are drawn off. Stream 405 is a fairly pure glycerol waste stream (96.4% glycerol, 2.8% ethanol, 0.6% water, and 0.2% other), and Stream 406 largely consists of biodiesel and unreacted oil (90.0% biodiesel, 8.3% oil, 1.7% other) and is sent to a secondary flash S-402 to remove additional impurities then to distillation column T-402 for final purification. The stream table is shown in Table 4-4-06.

The secondary flash S-402 takes in Stream 406. Pressure is dropped to atmospheric and occurs adiabatically. Stream 407 is the vapor stream which has been condensed for handling as waste and contains ethanol, biodiesel, glycerol, and water, so there's a small loss of biodiesel, but this increases purity after distillation by about 1.5% to reach 99.7% final purity, so it's necessary. Stream 408 is the liquid stream containing biodiesel and oil and is sent to distillation column T-402. Stream table is shown in Table 4-4-08.

Distillation column T-402 is run in vacuum conditions (0.05 bar) to lower the reboiler temperature to prevent oil/biodiesel decomposition at high temperatures, and it takes Stream 408 as input. Stream 409 is the purified biodiesel product, 99.7% biodiesel by mass, which is brought back to atmospheric pressure using the product pump P-404, and Stream 410 is the unreacted oil recycle which does not need its pressure changed as the incoming oil from lipid extraction is also at 0.05 bar. Additionally, this tower has a reflux pump P-406 whose specifications are described in Section 4.4.4.

Table 4-4-06: Two-phase Gravity Settler S-401 Mass Flows

Stream Number	404	405	406
Temperature (°C)	271	276	276
Pressure (bar)	7	7	7
Ethanol (kg/day)	800	150	650
Water (kg/day)	50	40	10
Glycerol (kg/day)	5200	4900	300
Biodiesel (kg/day)	53100	~0	53100
Algal Oil (kg/day)	4900	0	4900

Table 4-4-07: Two-phase Gravity Settler S-401 Specifications

Diameter (m)	3
Length (m)	4
MOC	316SS

Table 4-4-08: Secondary Flash Drum S-402 Mass Flows

Stream Number	406	407	408
Temperature (°C)	276	86	273
Pressure (bar)	7	1.01	1.01
Ethanol (kg/day)	650	550	100
Water (kg/day)	10	9	1
Glycerol (kg/day)	300	250	50
Biodiesel (kg/day)	53100	800	52300
Algal Oil (kg/day)	4900	0	4900

Table 4-4-09: Secondary Flash Drum S-402 Specifications

Diameter (m)	1
Length (m)	2
MOC	CS

Table 4-4-10: Biodiesel Purification Column T-402 Mass Flows

Stream Number	408	409	410
Temperature (°C)	273	86	333
Pressure (bar)	1.01	1.01	0.05
Ethanol (kg/day)	100	100	0
Water (kg/day)	1	1	0
Glycerol (kg/day)	50	50	0
Biodiesel (kg/day)	52300	52100	200
Algal Oil (kg/day)	4900	0	4900

Table 4-4-11: Biodiesel Purification Column T-402 Specifications

Stages	17 (15 trayed stages)	Height (m)	9
Condenser	Total	Diameter (m)	2
Reflux Ratio	1.5	MOC	CS
Feed Stage	7	Tray efficiency	0.55

Table 4-4-12: Biodiesel Purification Column Condenser E-406 and Reboiler E-407

	Condenser E-406	Reboiler E-407
Duty (kW)	-890	630
Area (m ²)	19.1	19.9

4.4.4 Ancillary Equipment

The designs of the two reactor stream heaters and pumps E-401 and E-402 and P-401 and P-402, fired heater H-401 and heating loop pump P-403, ethanol recycle stream condenser E-403, ethanol waste stream condenser E-408, product pump P-404, and tower reflux pumps P-405 and P-406 (for T-401 and T-402, respectively) are located below in their respective tables, organized by equipment type.

Worthy of clarification is the heating loop. Since the oil and ethanol streams need to be heated to 340°C, steam is not an ideal heat transfer fluid. Instead, a closed loop (depicted as dashed lines in Figure 4-4-01) containing a synthetic heat transfer fluid Therminol 68 is used for heating purposes (Eastman Chemical Company, 2015). The fired heater raises the temperature of the fluid up to 360°C, which is run through all the heat exchangers used for heating/reboilers before being brought back up to pressure by pump P-403 and run through the heater again.

Table 4-4-13: Biodiesel Heat Exchangers

	Duty (kW)	Area (m ²)	MOC
E-401	370	8.0	316SS
E-402	1100	25.9	316SS
E-403	490	8.6	316SS
E-408	630	19.9	316SS

Table 4-4-14: Biodiesel Pumps

	Flow rate (m ³ /s)	Shaft work (kW)	MOC
P-401	0.000743	18.0	316SS
P-402	0.001410	33.8	316SS
P-403	0.063300	31.6	CS
P-404	0.000736	0.101	CS

Table 4-4-15: Fired Heater

	Duty (kW) - 70% efficient	MOC
H-401	3700	CS

4.5 Fermentation Pretreatment

The process flow diagram for fermentation pretreatment is displayed in Figure 4-5-01.

Pump and heat exchanger specifications are found in Table 4-5-01. The component processes of Neutralization, Evaporation, and Rotary Vacuum Drum Filtration will be described individually in Sections 4.5.1-4.5.3.

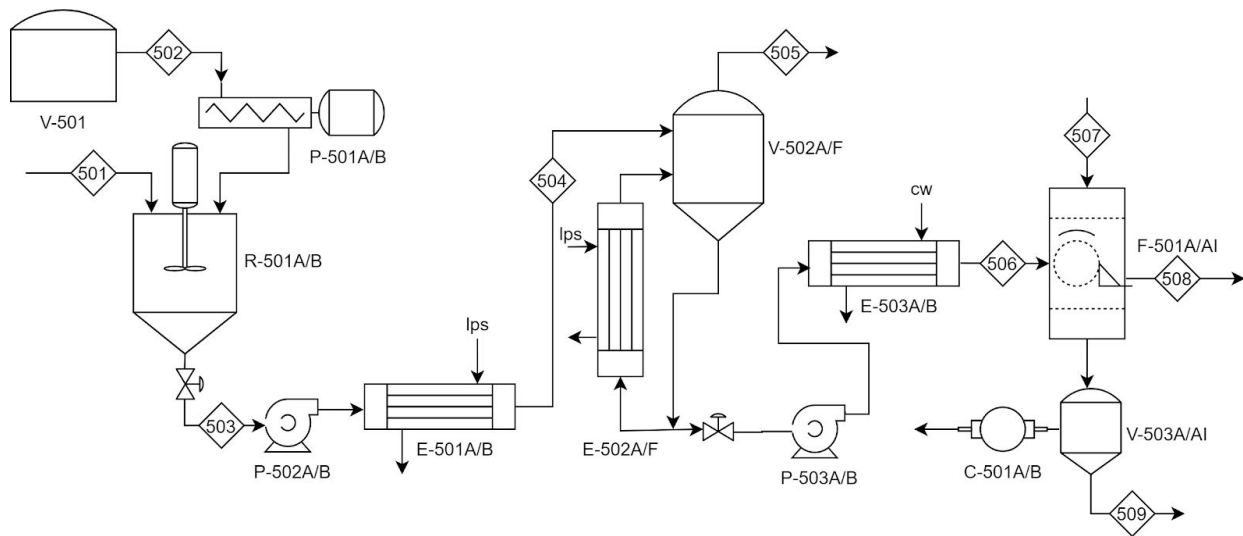


Figure 4-5-01: Fermentation Pretreatment Process Flow Diagram

Table 4-5-01: Fermentation Pretreatment Equipment Specifications; Note Vapor-Liquid Settler V-502A/F and Vacuum Trap V-503A/AI are omitted as ancillary equipment to the evaporator and vacuum filtration, while Neutralization Reactor R-501A/B and F-501A/AI are specified in Tables 4-5-03 and 4-5-06 respectively

Heat Exchangers	E-501A/B (1 operating)	E-502A/F (3 operating)	E-503A/B (1 operating)	
Type	Fl.H.	Fl.H.	Fl.H.	
Area (m ²)	172	851	253	
Heat Duty (MW)	34.6	252.4	-4.48	
Shell				
Temp (°C)	143.6	143.6	45	
Pressure (barg)	3	3	0.5	
MOC	CS	CS	CS	
Tube				
Temp (°C)	99	100	100	
Pressure (barg)	1	0	1	
MOC	316SS	316SS	316SS	
Pumps/ Compressors	P-501A/B	P-502A/B	P-503A/B	C-501A/B
Type	Screw	Centrifugal	Centrifugal	Steam Jet Ejector
Flow (kg/s)	1.74	130.6	19.5	0.243
Density (kg/m ³)	2210	977	1212	0.388
Shaft Power (kW)	1.60	19.1	2.29	0.129 kg steam/second*
Efficiency (%)	70	70	70	
Pressure in (barg)	0.5	0.5	0	-0.68
Pressure out (barg)	0.5	1.5	1	0
Temp (°C)	30	41.3	100	35
MOC	CS	316SS	316SS	CS

4.5.1 Neutralization

The lipid-extracted algae-sulfuric acid mixture (Stream 302) enters the continuous-stirred tank Neutralization Reactor R-501A/B. Solid calcium hydroxide is fed into the reactor from Base Storage V-501 with the Solid Conveyor P-501A/B. The storage is 2250 m³, to contain a 30 day supply of calcium hydroxide. The streams are mixed in the baffled Neutralization Reactor R-501A/B by a four pitched-blade turbine at 51 rpm with a residence time of 5 minutes. Calcium sulfate dihydrate (gypsum) crystals form as the mixture is neutralized. Two reactors are present so that maintenance may be regularly performed to remove gypsum scaling.

Table 4-5-02: Neutralization Mass Flows

Stream Number	501	502	503
Temperature (°C)	35	30	41.3
Pressure (bar)	1.5	1.01	1.01
Water (kg/day)	10,765,700	0	10,771,800
Ca(OH) ₂ (s) (kg/day)	0	150,300	0
H ₂ SO ₄ (kg/day)	199,000	0	<10 ⁻²
CaSO ₄ (aq) (kg/day)	0	0	22,300
CaSO ₄ *2H ₂ O (s) (kg/day)	0	0	320,300
Glucose (aq) (kg/day)	72,700	0	72,700
Algae Waste (aq) (kg/day)	94,000	0	94,000

Table 4-5-03: Neutralization Reactor R-501A/B Specifications

Diameter (m)	4	Impeller	Four Pitched-Blade Turbine
Height (m)	4	Impeller Diameter (m)	1.33
Residence Time (s)	300	Baffles	4
Pressure (barg)	0.5	Baffle Size (m)	0.33
Temperature (°C)	41.3	Impeller PRM	51
MOC	316SS	Mixing Power (kW)	3.36

4.5.2 Evaporation

Evaporator Pump P-502A/B brings the neutralized liquid-solid mixture to 1.5 barg to drive it through the Evaporation Preheater E-501A/B and into Evaporator E-502A/F. Three evaporators are operated at any time of six total to allow maintenance for gypsum scaling. The mixture is brought to 99°C by the shell-and-tube preheater before being fed into the evaporators' Vapor-Liquid Settler V501A/F. The downcoming liquid-solid mixture is fed back into the vertical long-tube Evaporator E-502A/F, with a portion of the mixture bled off as the concentrated slurry product. The evaporator removes about 89% of the water, concentrating the glucose solution for fermentation.

Table 4-5-04: Evaporation Mass Flows

Stream Number	504	505	506
Temperature (°C)	99	100	30
Pressure (bar)	1.5	1.01	1.01
Water (kg/day)	10,771,800	9,601,200	1,165,200
CaSO ₄ (aq) (kg/day)	22,300	0	2,600
CaSO ₄ *2H ₂ O (s) (kg/day)	320,300	0	346,000
Glucose (aq) (kg/day)	72,700	0	72,700
Algae Waste (aq) (kg/day)	94,000	0	94,000

4.5.3 Rotary Vacuum Drum Filtration

Slurry Pump P-503A/F pumps the 21% solid by weight mixture to 2 barg to drive it through the Evaporator Cooler E-503A/B and feed it to the Gypsum Filter F-501A/AI. The shell-and-tube Evaporator Cooler E-503A/B brings the slurry to 30°C. The rotary vacuum drum Gypsum Filter F-501A/AI operates at 5 minutes per rotation, with 35% of the surface submerged. Of the 35 drums, 25 operate at any time. A gypsum cake of 9.8 mm forms on the surface of the drums, with 3.8 mm removed per rotation leaving 6 mm for filtration. Water washes the exposed surface of the drum to recover most of the entrained glucose solution. A vacuum of 0.338 bar is drawn by Vacuum Compressor C-501A/B, for a pressure differential of 0.676 bar, to draw the filtrate into the Vacuum Trap V-503A/AI where air is separated. The liquid Stream 509 continues to fermentation.

Table 4-5-05: Rotary Vacuum Drum Filtration Mass Flows

Stream Number	506	507	508	509
Temperature (°C)	30	30	30	30
Pressure (bar)	1.01	1.01	1.01	0.33
Water (kg/day)	1,165,200	518,400	297,200	1,386,600
CaSO ₄ (aq) (kg/day)	2,600	0	700	2,600
CaSO ₄ *2H ₂ O (s) (kg/day)	346,000	0	345,200	0
Glucose (aq) (kg/day)	72,700	0	1,300	71,400
Algae Waste (aq) (kg/day)	94,000	0	47,000	47,000

Table 4-5-06: Rotary Vacuum Drum Filtration F-501A/AI Specifications (per drum)

Length (m)	2	Cake removed (m)	0.0038
Diameter (m)	2	Cake left behind (m)	0.0060
Surface Area (m ²)	12.6	ΔP (bar)	0.68
RPM	0.2	Air intake (m ³ /s)	0.0038
Wash Ratio	1.5	MOC	CS/cloth

4.6 Fermentation and Ethanol Purification

4.6.1 Continuous Fermentation

The stream pumped into the fermenting drums is the same as that which is exiting the rotary vacuum filter drum. Stream 1 enters at 47.6 g/L glucose at 62.5 m³/hr. This is split such that half the volume enters R-601, and the other half is split between R-602 and R-603. This ensures that there is still sugar available for the yeast to ferment in all the fermenters. Pumps P-602 and P-603 move the fermentation broth from one fermenter to the next, ensuring suspension of yeast by flowing the solution. Since the dilution rate is so low, each reactor is able to work to near completion. This means the sugar content in stream 2 is near zero. The total residence time is 19.5 hours and the final concentration of ethanol is 3.2% by volume.

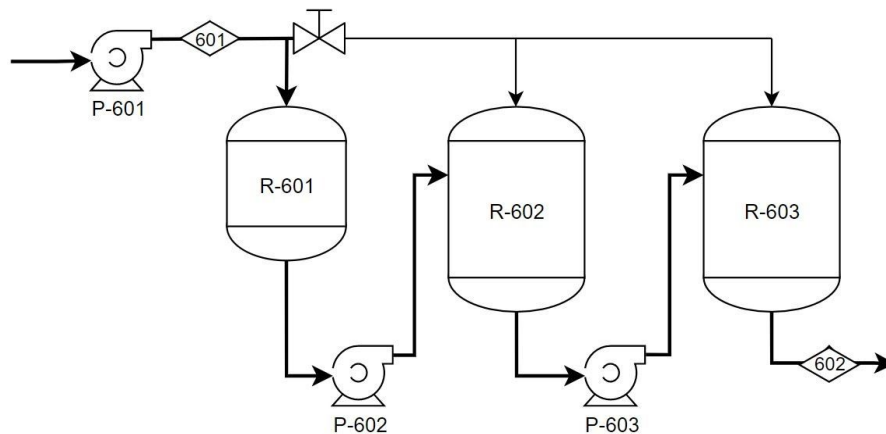


Figure 4-6-01: Continuous Fermentation Process Flow Diagram

Table 4-6-01: Continuous Fermentation Mass Flows

Stream	601	602
Temperature (°C)	30	30
Pressure (bar)	1.01	1.01
Water (kg/day)	1,500,000	1,500,000
Ethanol (kg/day)	0	37,700
Glucose (kg/day)	71,400	~0
Solids (kg/day)	50,000	84,700

Table 4-6-02: Continuous Fermentation Specifications

	R-601	R-602	R-603
Height (m)	11	15	15
Diameter (m)	5.5	7.5	7.5
Volume (m ³)	200	350	350
Dilution Rate (1/hr)	0.154	0.134	0.179
Residence Time (hr)	6.4	7.47	7.47
MOC	316SS	316SS	316SS

4.6.2 Solids Separation

Passing stream 2 through the centrifugal separators S-602 and S-603, the creates a liquid stream with exclusively water and ethanol (stream 3) and a slurry stream with all the solids and some liquid (stream 4). The decanter centrifuges removes the solids in a slurry which is 40% solids by mass. This resultant slurry does contain some ethanol, but the recovery equipment needed to retrieve it is not worth the quantity of ethanol that could be recovered. Total Power cost is 156 kW per decanter.

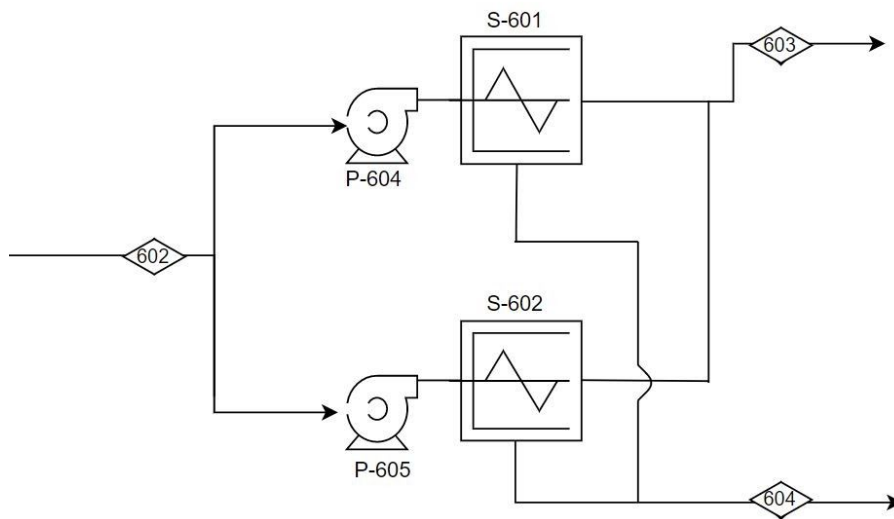


Figure 4-6-02: Decanter Centrifuges Process Flow Diagram

Table 4-6-03: Solids Separation Mass Flows

Stream	602	603	604
Temperature (°C)	30	30	30
Pressure (bar)	1.01	1.01	1.01
Water (kg/hr)	200,000	17,200	182,800
Ethanol (kg/hr)	5,030	430	4,600
Solids (kg/hr)	11,450	11,450	0

Table 4-6-04: Solids Separation Specifications

Diameter (m)	Speed (rpm)	G force	Main Motor (kW)	Back Motor (kW)	Capacity (m ³ /hr)	Weight (kg)	Dimensions (m)
720	2200	1951	130	26	100	9000	6×3.25×1.5

4.6.3 Distillation to Azeotrope

The distillation column takes the dilute 3% water ethanol solution and refines it to a near azeotropic concentration of 95.5%. The number of theoretical stages calculated was 20 so assuming an efficiency of 70 percent meant there were more required. A 30 stage distillation column was used that uses a bottoms feed heat exchanger to preheat the solution. There are two reboilers at the bottom of the column, E-602a and E-602b, which are designed so that only one is being run at a time. The second one is present so that when organic matter enters then burns onto the reboiler, then they can be switched without halting operation.

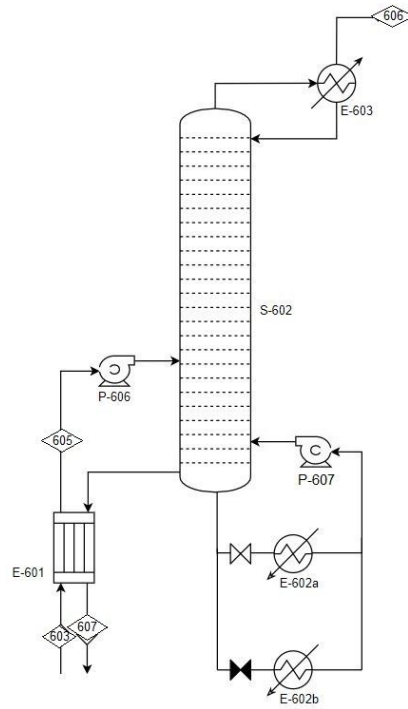


Figure 4-6-03: Ethanol Distillation Process Flow Diagram

Table 4-6-05: Azeotropic Distillation Mass Flows

Stream	603	606	607
Temperature (°C)	30	79	87
Pressure (bar)	1.01	1.01	1.01
Water (kg/hr)	182,829	273	182,556
Ethanol (kg/hr)	4,595	4,595	~0

Table 4-6-06: Azeotropic Distillation Specifications

Diameter (m)	Height (m)	Trays	Reflux ratio	Condenser Duty (MW)	Reboiler Duty (MW)	Feed- bot Exchanger	MOC
0.8	15	30	29.7	42	52	13.7	316SS

4.6.4 Azeotrope Breaking

Azeotrope breaking starts with the 95.5% ethanol solution created during the distillation and rectifying that to 99.5%, or the fuel grade. There are two zeolite adsorption columns containing 8000 kg of an aluminosilicate catalyst. One is pulling the water from the ethanol vapors and the other is recharging using dry air, stream 8, to encourage water to leave. The valves are oriented in Figure 4-6-04 such that S-603a (left) is absorbing water and S-603b (right) is recharging. Stream 9 is the fuel grade ethanol exiting while stream 10 is the air after it has taken water back from the zeolite bed. The adsorbing column operates at 80°C in order to keep the ethanol-water azeotrope in its vapor phase. The total run time for each column will be 3.75 hours, alternating every 40 minutes.

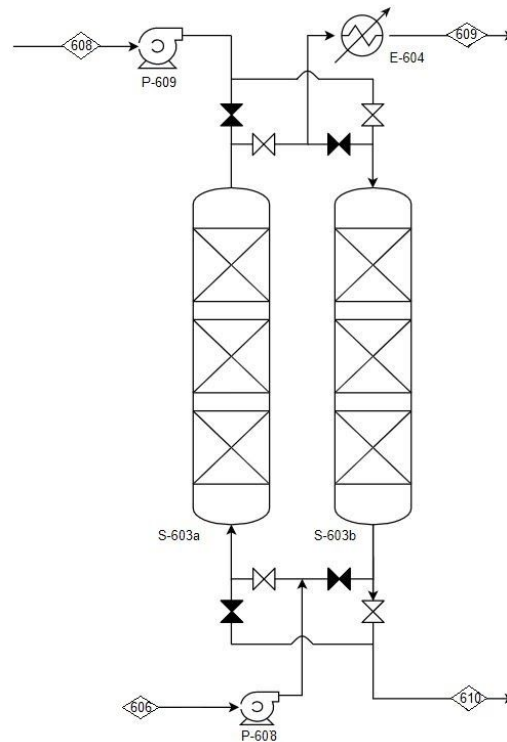


Figure 4-6-04: Azeotrope Breaking Process Flow Diagram

Table 4-6-07: Azeotropic Breaking Mass Flows

Stream	606	608	609	610
Temperature (°C)	87	30	82	30
Pressure (bar)	1.01	1.01	1.01	1.01
Water (kg/hr)	273	54	29.4	540
Ethanol (kg/hr)	4,595	0	4,595	0
Air (m ³ /hr)	0	20,820	0	20,820

Table 4-6-08: Azeotropic Breaking Specifications

	Adsorbing Column	Recharging Column
Residence time (s)	19	21
Height (m)	8.72	8.72
Diameter	4.4	4.4
MOC	316SS	316SS

The final product is ethanol but that is not the only stream that is exiting the system that is a result of the production. The first waste stream is a decanted slurry (604) that is forty percent by mass solids, primarily yeast but also some algal remains. This stream could potentially be sold as an organic slurry for livestock, however it is being treated as a harmless waste stream that will cost nothing to get rid of. The next stream is hot water coming off of the bottoms from distillation (607). It will have to be cooled to a lower temperature before dumping. The final waste stream is the wet air after the zeolite column is recharged (610). This humid air can be released to the environment because it is not dangerous thermally or otherwise.

Table 4-6-09 Ethanol Production Ancillary Equipment- Pumps and Compressors

Pumps/ Compressors	P-601	P-602	P-603	P-604/605	P-606	P-607	P-608	C-609
Type	Centrif.	Centrif.	Centrif.	Centrif.	Centrif.	Centrif.	Centrif.	Comp.
Flow (m ³ /hr)	62.5	31.25	46.88	100	100	97	100	20820
Shaft Power (kW)	9.37	4.68	7.02	14.99	14.99	9.3	14.99	3.82
Efficiency (%)	70	70	70	70	70	70	70	60
Pressure in (barg)	1.1	1.1	1.1	1.1	1.1	1.8	1.5	1.1
Pressure out (barg)	1.6	2.1	1.6	1.6	2.5	2.3	2.8	2.6
Temp (°C)	30	30	30	30	79	119	87	30
MOC	316SS	316SS	316SS	316SS	316SS	316SS	316SS	316SS

5. Economic Analysis

Purchased equipment, utility, and material costs are evaluated by process section. Total capital costs and operating costs, including labor, taxes, and insurance, are evaluated for the entire process.

5.1 Equipment Purchase and Operating Costs

5.1.1 Algae Cultivation and Harvesting

The capital cost for algae cultivation and harvesting can be divided into 3 parts: the cost of the land, the cost of building the raceways, and the cost of the rest of the processing equipment. Land was priced using prices available by the Real Estate Center at Texas A&M. The price listed below is the price of land in the Texas Northeastern region, in the fourth quarter of 2019. 8.5 square miles of land will be bought, 8.25 square miles of which will be utilized for algae cultivation.

Table 5-1-01: Cost of Land

Land cost (\$/acre)	4843
Acres	5440
Total Cost (\$)	26,345,920

The cost of building the open pond raceways was determined by using data available for the cost of hiring a contractor to build a pond (*2020 Costs to Build a Pond —HomeAdvisor*, n.d.).

Table 5-1-02: Cost of Building Raceways

Pond Making Cost (\$/acre)	3000
Total Acres	5,019
Total Cost (\$)	15,057,120

In addition to the cost of building the ponds, the price of 2 cm thick PVC liner was added. Enough liner will be bought to line all sides of the raceways, and make a mid raceway divider. The price of PVC liner was obtained from AliBaba (2020).

Table 5-1-03: Cost of PVC Liner

PVC Cost (\$/ton)	800
Density (kg/m ³)	1.4
Thickness (m)	0.02
Total area (m ²)	21,254,720
Tons Needed	595
Total PVC Cost (\$)	\$476,106

The purchased equipment price of the remaining processing equipment, other than the sedimentation tanks, was determined using Peters et al. (2013) and adjusted using a CEPCI of 596.1.

Table 5-1-04: Purchased Equipment Pricing of Algae Cultivation

Equipment	Size	Price (\$, 2001)	MOC Factor	CEPCI Factor	Quantity	Price (\$)
P-101	0.926 m ³ /s	20,000	2.4	1.502	50	3,603,627
P-102	0.463 m ³ /s	16,000	2.4	1.502	100	5,765,804
P-103	0.001 m ³ /s	1,200	6	1.502	2	21,622
M-101	97 kW	90,000	1	1.502	62	8,378,433
P-104	0.62 m ³ /s	15,000	2.4	1.502	2	108,109
Total						17,877,595

The sedimentation tanks were priced using a report published by the National Service Center for Environmental Publications (NSCEP) on the cost of wastewater treatment processes (Robert A. Taft Water Research Center, 1968). The correlation below was used to relate the area of settling tanks to cost, and the cost was then adjusted using CEPCI of 596.1.

$$\text{Log (Cost)} = \frac{1}{0.233\text{Log(Area)} + 0.758}$$

In this equation, area is in units of thousand sq. ft and cost in dollars/sq. ft.

Table 5-1-05: Purchased Equipment Cost of Sedimentation Tanks

Equipment	Size	Price (\$, 1968)	CEPCI Factor	Quantity	Price (\$)
R-102	3850 m ²	315,000	5.243	6	9,909,000

The operating costs for the algae cultivation and harvesting section consists of the cost of ferric chloride, and the electricity costs associated with pumping and mixing for various unit operations.

Table 5-1-06: Operating Cost of Algae Cultivation and Harvesting

Operation	Material	Amount	Cost	Cost (\$/year)
Stream 103	Ferric Chloride	125 tons/day	150 \$/ton	6,843,750
P-101	Electricity	14694 kW	18.72 \$/GJ	8,674,923
P-102	Electricity	18388 kW	18.72 \$/GJ	10,855,953
P-103	Electricity	162 W	18.72 \$/GJ	96
P-104	Electricity	393 kW	18.72 \$/GJ	232,206
R-101	Electricity	1704 kW	18.72 \$/GJ	1,006,225
M-101	Electricity	6665 kW	18.72 \$/GJ	3,934,709
Total				31,548,000

5.1.2 Algae Pretreatment

The purchased equipment costs were estimated using Figures from Chapters 12 and 14 of Peters et al. (2003), and adjusted to the 2019 CEPCI of 596.1.

Table 5-1-07: Purchased Equipment Cost for Algae Pretreatment

Equipment	Size	Price (\$, 2001)	MOC Factor	CEPCI Factor	Quantity	Price (\$)
P-201	0.00128 m ³	1,400	2.4	1.502	2	10,100
P-202	0.126 m ³	8,500	2.4	1.502	2	61,300
E-201A/B	1036 m ²	70,000	3	1.502	2	630,600
E-202	345 m ²	30,000	1.7	1.502	1	76,600
E-203A/B	701 m ²	50,000	1.7	1.502	2	255,300
R-201	0.5x790 m	1,185,000	1.25	1.502	1	2,224,100
R-201 (insulation)	0.5 inch, 0.5x790 m	395,00	1	1.502	1	59,300
V-201	3600 m ³	230,000	3	1.502	1	1,036,000
Total						4,353,300

The operating cost for this subprocess is a sum of material and utility costs. The only material cost is the sulfuric acid homogeneous catalyst. Utility cost is composed of electricity, cooling water, and steam costs. Costs were retrieved from Alibaba and Turton (2018) Table 8.3. The largest cost for this subprocess by far is the sulfuric acid catalyst, at almost 90% of the operating cost.

Table 5-1-08: Operating Costs for Algae Pretreatment

Operation	Material	Amount	Cost	Cost (\$/year)
Stream 502	H ₂ SO ₄	199.0 tons/day	200 \$/ton	14,527,000
E-202	mps	538.8 tons/day	9.61 \$/ton	1,539,000
E-203A/B	cw	14,910 tons/day	15.7 \$/1000 m ³	85,000
P-201	Electricity	0.899 kW	18.72 \$/GJ	500
P-202	Electricity	80.31 kW	18.72 \$/GJ	47,400
Total				16,198,900

5.1.3 Lipid Extraction

The purchased equipment costs were estimated using Figures from Chapters 12 and 14 of Peters et al. (2003), and adjusted to the 2019 CEPCI of 596.1. Hexane is included because a large amount must be initially purchased for the facility to start operating normally. The recycle stream recovers nearly all of the hexane, so very little makeup hexane will be required to continue normal operations.

Table 5-1-09: Purchased Equipment Costs and Initial Material Cost for Lipid Extraction

Equipment or Component	Size (m ³)	Price (\$, 2001)	MOC Factor	CEPCI Factor	Quantity	Price (\$)
S-301A/B	285	159,000	1.8	1.502	2	991,000
E-301	75	381,000	1.8	1.502	1	667,000
C-301	0.02	12,000	2.4	1.502	2	27,400
P-301	0.15	10,630	2.4	1.502	2	24,200
P-302	0.02	8,960	2.4	1.502	2	20,400
Hexane	-	-	-	-	1,000,000 kg	550,100
Total						2,280,100

The operating cost for this section of the facility is a sum of the material and utility costs. The only material cost is makeup hexane, due to a small amount of hexane which is not able to be recycled each day. The utility cost is solely electricity. All costs are taken from Alibaba and Turton (2018) Table 8.3. S-301A/B is not included in utility calculations because it requires no utility input; the separation of lipids and hexane from the rest of the mixture is done with their differing polarities.

Table 5-1-10: Operating Costs for Lipid Extraction

Operation	Material	Amount	Cost	Cost (\$/year)
Stream 301	Hexane	34 kg/day	\$50/ton	700
E-301	lps	566.38 ton/day	\$9.45/ton	1,953,586
C-301	Electricity	2.215 kW	18.72 \$/GJ	1,306
P-301	Electricity	7.233 kW	18.72 \$/GJ	4,250
P-301	Electricity	3.909 kW	18.72 \$/GJ	2,300
Total				1,962,142

5.1.4 Biodiesel Production and Purification

The purchased equipment costs were estimated using Figures from Chapters 12 and 14 of Peters et al. (2003) as well as the CAPCOST program by Turton (2018), and adjusted to the 2019 CEPCI of 596.1.

Table 5-1-11: Purchased Equipment Cost for Biodiesel Production and Purification

Equipment	Sizing/ Capacity	Price (\$, 2001/2016)	MOC/P-T Factor	CEPCI Factor	Quantity	Price (\$)
P-401	0.000760 m ³ /s	1,200	7.92	1.502	2	28,500
P-402	0.001426 m ³ /s	1,500	7.92	1.502	2	35,700
P-403	0.0633 m ³ /s	6,000	1	1.502	2	18,000
P-404	0.000763 m ³ /s	1,200	1	1.502	2	3,600
P-405	0.00134 m ³ /s	1,500	1	1.502	2	4,500
P-406	0.00184 m ³ /s	1,500	1	1.502	2	4,500
E-401	8.06 m ²	4,000	1.2	1.502	1	7,200
E-402	25.9 m ²	8,000	1.2	1.502	1	14,400
E-403	15.2 m ²	4,500	1.7	1.502	1	11,500
E-404	8.6 m ²	4,000	1.7	1.502	1	10,200
E-405	9.8 m ²	4,000	1.7	1.502	1	10,200
E-406	19.8 m ²	5,500	1	1.502	1	8,300
E-407	19.1 m ²	5,500	1.7	1.502	1	14,000
E-408	0.167 m ²	1,900	1	1.502	1	2,800
R-401	12.6 m ³	1,870,000	1	1.10	1	2,057,000
T-401	4.1 m ³	71,600	1	1.10	1	58,200
T-402	28.5 m ³	84,100	1	1.10	1	68,400
S-401	28.3 m ³	207,000	1	1.10	1	228,000
S-402	1.6 m ³	5,300	1	1.10	1	5,800
H-401	4 MW	1,066,000	1	1.10	1	1,170,000
Total						3,800,000

The most costly pieces of equipment are the reactor R-401 (due to the 170 bar reaction pressure), fired heater H-401, and gravity settler S-401 due to long residence time. The alternative to a large settling vessel would be to centrifuge the biodiesel-glycerol mixture, but that would involve some amount of energy expenditure over time.

The operating cost for this process is the sum of utility costs as the only material inputs are algae oil and ethanol, both of which are produced on-site. Utility costs come from cooling water, electricity, and natural gas to power the fired heater and are sourced from Turton Table 8.3 and the U.S. EIA (Turton, 2018; U.S. Energy Information Administration, 2020). Natural gas price has been converted from \$/1000 ft³ to \$/GJ for easier comparison with electricity price. Additionally, burning the small mixed waste stream (Stream 407) can produce about 0.5 MW of energy when used as fuel for the furnace, saving about \$40,000/year in energy costs.

Table 5-1-12: Operating Costs for Biodiesel Production and Purification

Operation	Material	Amount	Cost	Cost (\$/year)
E-403	cw	1296 tons/day	15.7 \$/1000 m ³	7,400
E-405	cw	1296 tons/day	15.7 \$/1000 m ³	7,400
E-407	cw	1296 tons/day	15.7 \$/1000 m ³	7,400
E-408	cw	86.4 tons/day	15.7 \$/1000 m ³	500
R-01	cw	550 tons/day	15.7 \$/1000 m ³	3,200
P-401	Electricity	20.0 kW	18.72 \$/GJ	12,000
P-402	Electricity	37.6 kW	18.72 \$/GJ	22,000
P-403	Electricity	35.2 kW	18.72 \$/GJ	21,000
P-404	Electricity	0.112 kW	18.72 \$/GJ	100
P-405	Electricity	0.023 kW	18.72 \$/GJ	10
P-406	Electricity	0.012 kW	18.72 \$/GJ	10
<i>H-401 (no waste)</i>	<i>Natural gas</i>	<i>3.7 MW</i>	<i>2.62 \$/GJ</i>	<i>310,000</i>
H-401 w/ waste	NG, waste fuel	3.2 MW	2.62 \$/GJ	270,000
Total				350,000

5.1.5 Fermentation Pretreatment

The purchased equipment costs were estimated using Figures from Chapters 12, 14, and 15 of Peters et al. (2003), and adjusted to the 2019 CEPCI of 596.1. The evaporator and drum filter are the largest purchase costs by far, partially due to having a large number of operating units. Capital costs can be thus greatly reduced by eliminating the gypsum scaling in the evaporators, and by sourcing larger drum-filters.

Table 5-1-13: Purchased Equipment Cost for Fermentation Pretreatment

Equipment	Size	Price (\$, 2001)	MOC Factor	CEPCI Factor	Quantity	Price (\$)
P-501A/B	0.23x10m	7,500	1	1.502	2	22,500
P-502A/B	0.134 m ³ /s	9,000	2.4	1.502	2	64,900
P-503A/B	0.016 m ³ /s	2,500	2.4	1.502	2	18,000
C-501	0.0366 kg/s	5,500	1	1.502	2	8,300
E-501A/B	438 m ²	34,000	1.7	1.502	2	173,600
E-502A/F	851 m ²	620,000	2.1	1.502	6	11,729,800
E-503A/B	253 m ²	23,000	1.7	1.502	2	117,400
R-501	50 m ³	80,000	1	1.502	2	240,200
F-501A/AI	12.6 m ²	140,000	1.5	1.502	35	11,036,100
V-501	2250 m ³	130,000	1	1.502	1	195,200
Total						23,606,000

The material costs for this subprocess are calcium hydroxide, washing water, and solid-cake disposal, treated as nontoxic waste. Utility cost is composed of electricity, cooling water, and steam costs. Costs were retrieved from Alibaba and Turton (2018) Table 8.3. The largest cost is the evaporator steam, which may be reduced by using multiple effects (see Section

5.3.3). The calcium hydroxide purchase and gypsum disposal also comprise major costs, less easily mitigated.

Table 5-1-14: Operating Costs for Fermentation Pretreatment

Operation	Material	Amount	Cost	Cost (\$/year)
Stream 502	Ca(OH) ₂	150.3 tons/day	100 \$/ton	5,486,000
Stream 507	H ₂ O	518.4 tons/day	0.177 \$/ton	33,500
Stream 508	Gypsum, H ₂ O	691.4 tons/day	36 \$/ton	9,085,000
E-501A/B	lps	1,401 tons/day	9.45 \$/ton	4,832,000
E-502A/F	lps	10,156 tons/day	9.45 \$/ton	35,032,000
E-503A/B	cw	6,158 tons/day	15.7 \$/1000 m ³	35,300
P-501A/B	Electricity	1.78 kW	18.72 \$/GJ	1,100
P-502A/B	Electricity	21.2 kW	18.72 \$/GJ	12,500
P-503A/B	Electricity	2.55 kW	18.72 \$/GJ	1,500
C-501A/B	lps	11.2 tons/day	9.45 \$/ton	38,600
Total				54,558,000

5.1.6 Fermentation and Ethanol Purification

The purchased equipment was calculated using figures Chapters 12, 14, and 15 of Peters et al. (2003) as well as CAPCOST 2017. All the prices were scaled to the 2019 CEPCI of 596.1. The largest equipment costs were the fermenters, distillation tower, zeolite columns, and dry air compressor.

Table 5-1-15: Purchased Equipment Cost for Ethanol Fermentation and Purification

Equipment	Size	Price (\$, 2001)	MOC Factor	CEPCI Factor	Quantity	Price (\$)
P-601	0.0174 m ³ /s	\$2,430	1.8	1.50	2	\$13,137
P-602	0.0087 m ³ /s	\$1,943	1.8	1.50	2	\$10,501
P-603	0.0130 m ³ /s	\$2,187	1.8	1.50	2	\$11,819
P-604/605	0.0278 m ³ /s	\$3,016	1.8	1.50	2	\$16,300
P-606	0.0278 m ³ /s	\$3,016	1.8	1.50	2	\$16,300
P-607	0.0270 m ³ /s	\$2,968	1.8	1.50	2	\$16,041
P-608	0.0278 m ³ /s	\$3,016	1.8	1.50	2	\$16,300
C-609	5.78 m ³ /s	\$326,373	1	1.50	4	\$659,229
E-601	13.7 MW	\$26,200	1.8	1.50	1	\$28,815
R-601	200 m ³	\$709,109	1	1.10	1	\$779,889
R-602	350 m ³	\$1,226,159	1	1.10	1	\$1,348,548
R-603	350 m ³	\$1,226,159	1	1.10	1	\$1,348,548
S-601/602	0.0278 m ³ /s	\$150,000	1	1	2	\$300,000
S-603	30.2 m ³	\$2,837,509	1	1.10	1	\$3,120,736
S-604A/B	6.9 m ³	\$336,000	1	1.10	2	\$1,009,015
Total						\$8,882,218

The largest operational cost is the reboiler steam needed for creating the water ethanol azeotrope. It was recommended to use a feed-bottoms exchanger which reduced reboiler duty by 18%, a significant decrease. The next largest operational cost was the decanter centrifuge which costs an order of magnitude less than the reboiler.

Table 5-1-16: Operating Costs for Ethanol Production

Operation	Material	Amount	Cost	Cost (\$/year)
S-603 reboil	lps	2,117 tons/day	9.45 \$/ton	\$2,294,927
S-603 condense	cw	57,801 tons/day	15.7 \$/1000 m ³	\$103,520
S-601/602	Electricity	156 kW	18.72 \$/GJ	\$28,779
P-601	Electricity	9.37 kW	18.72 \$/GJ	\$5,121
P-602	Electricity	4.68 kW	18.72 \$/GJ	\$2,558
P-603	Electricity	7.02 kW	18.72 \$/GJ	\$3,837
P-604/605	Electricity	14.99 kW	18.72 \$/GJ	\$3,072
P-606	Electricity	14.99 kW	18.72 \$/GJ	\$3,072
P-607	Electricity	9.3 kW	18.72 \$/GJ	\$1,906
P-608	Electricity	14.99 kW	18.72 \$/GJ	\$3,072
C-609	Electricity	3.82 kW	18.72 \$/GJ	\$783
Total				\$2,450,651

5.2 Total Capital and Operating Costs

5.2.1 Fixed Capital Costs

The total fixed capital cost is estimated in proportion to the purchased equipment costs. The factors were estimated with Peters et al. (2003) Table 6-9 for a fluid-processing plant. For algae cultivation, ie. the raceways, some of the costs were not included as contractors were hired to build plastic lined ponds. The factors used to estimate the capital cost are summarized in Table 5-2-01.

Table 5-2-01: Factors to Estimate Fixed Capital Cost from Purchased Equipment Cost

Item	Factor (Algal Raceways)	Factor (All Other Sections)
Equipment	1	1
Installation	-	0.47
Instrumentation/ controls	-	0.36
Piping	0.68	0.68
Electrical	0.11	0.11
Buildings	-	0.18
Yard improvements	0.1	0.1
Service Facilities	0.7	0.7
Engineering and supervision	-	0.33
Construction expenses	-	0.41
Legal	0.04	0.04
Contractor	-	0.22
Contingency	0.44	0.44
Fixed Capital	3.07	5.04

Table 5-2-02: Estimation of Capital Cost from Purchased Equipment Cost

Process Section	Purchased Eq. Cost (\$)	Fixed Capital Factor	Fixed Capital Cost (\$)
Alg. Harvesting	70,098,000	-	214,077,000
Land	26,346,000	1	26,346,000
Algae Raceways	15,533,000	3.07	47,687,000
Processing	27,787,000	5.04	140,044,000
Alg. Pretreatment	4,353,000	5.04	21,941,000
Lipid Extraction	2,280,100	5.04	11,492,000
Biodiesel Prod.	3,800,000	5.04	19,152,000
Ferm. Pretreatment	23,606,000	5.04	118,974,000
Ethanol Prod.	8,882,200	5.04	44,766,000
Total			430,402,000

5.2.2 Working and Total Capital Costs

Working capital is estimated as 15% of the total capital investment to account for stock of raw materials and finished products and cash on hand for expenses and fees. This capital is recovered at plant decommissioning. In reality, the amount of working capital may be larger due to the seasonal nature of the plant's operation.

Table 5-2-03: Summary of Total Capital Costs

Process Section	Fixed Capital (\$)	Working Capital (\$)	Total Capital (\$)
Alg. Harvesting	214,077,000	37,778,000	251,855,000
Alg. Pretreatment	21,941,000	3,872,000	25,813,000
Lipid Extraction	11,492,000	2,028,000	13,520,000
Biodiesel Prod.	19,152,000	3,376,000	22,528,000
Ferm. Pretreatment	118,974,000	20,995,000	139,969,000
Ethanol Prod.	44,766,000	7,890,000	52,666,000
Total	430,302,000	75,949,000	506,251,000

5.2.3 Operating Cost and Product Revenue

The process operating costs, including feedstock and utility costs, are summarized in Table 5-2-04. The product revenue is shown in Table 5-2-05.

Table 5-2-04: Operating Costs Summary

Process Section	Operating Cost (\$/year)
Alg. Harvesting	31,548,000
Alg. Pretreatment	16,199,000
Lipid Extraction	1,962,000
Biodiesel Prod.	350,000
Ferm. Pretreatment	54,558,000
Ethanol Prod.	2,451,000
Total	107,068,000

Table 5-2-05: Product Revenue

Product	Amount (gal/yr)	Price (\$/gal)	Income (\$/yr)
Ethanol	2,968,430	0.93	2,761,000
Diesel	6,132,000	3.72	22,811,000
Total			25,572,000

5.2.4 Labor Costs

The number of workers needed to operate the plant is estimated using Equation 8.3 from Turton (2018):

$$N_{OL} = (6.29 + 31.7P^2 + 0.23N_{np})^{0.5}$$

where N_{OL} is number of operators per shift, P is the number of particulate-handling steps, and N_{np} is the number of non-particulate handling steps (excluding pumps and vessels). For algae harvesting, each set of 10 raceways was counted as a fluid step. The values for the process are summarized in Table 5-2-04.

Table 5-2-06: Number of Process Steps

Process Section	Particulate Steps (P)	Fluid Steps (N_{np})
Alg. Harvesting	0	1084
Alg. Pretreatment	0	6
Lipid Extraction	2	3
Biodiesel Prod.	0	10
Ferm. Pretreatment	1	31
Ethanol Prod.	0	12
Total	3	1146

Values of 3 for P and 1146 for N_{np} correspond to 23.56 operators per shift. The adjustment from this to labor cost is performed in Table 5-2-05. The total number of operators employed is taken to be five times that per shift for continuous operation. Half of the workers are assumed to work in algae cultivation, where their salary is \$40,000, or \$19 per hour. The other half work in the processing steps, where their salary is \$67,000, or about \$32 per hour based on Turton (2018). The supervision costs are assumed to be an extra 15%, and healthcare and

retirement benefits are assumed to be an extra 50% cost on top of salaries. The labor costs are summarized in Table 5-2-05.

Table 5-2-07: Labor Costs

Operators per Shift	23.56
Total Operators	118
Average Salary	\$53,500
Supervisor Factor	1.15
Employee Benefits Factor	1.5
Total Labor Cost per Year	\$10,890,000

5.2.5 Taxes and Other Fees

Being on the outskirts of Houston, local property taxes are assumed to be 2% of the fixed capital investment per year, between values for dense and non-dense populated areas in Peters et al. (2003). This results in a yearly cost of \$8,608,000 on the fixed capital cost of \$430,402,000.

Similarly, insurance costs are estimated to be 1% of the fixed capital cost per year. This results in a yearly cost of \$4,304,000.

To estimate income tax, depreciation is estimated with the straight line method. The fixed capital investment of the plant is assumed to depreciate linearly over a 9.5 year recovery period, resulting in yearly depreciation of \$45,303,000. Total operating profit is subtracted by depreciation before taking income tax. Income tax is assumed to be 35%, for federal income tax and considering Texas does not have income tax (Peters et al., 2003). The current cash flow is negative, so no income tax is paid; however, in scenarios of higher fuel prices, income tax and depreciation become important factors.

5.2.6 Cash Flow Analysis

The operating cash flow is summarized in Table 5-2-07.

Table 5-2-08: Operating Cash Flow

Item	Cash Flow (\$/yr)
Plant Operation	-107,608,000
Labor	-10,890,000
Revenue	25,572,000
Property Tax	-8,608,000
Insurance	-4,304,000
Income Tax	0
Total	-105,838,000

The total plant lifespan is assumed to be 22 years. The plant is constructed over 18 months, wherein the total capital cost is spread uniformly. The first six months of start-up proceeds assuming half of revenue and plant operating costs, but full labor property tax, and insurance costs. For the next 20 years, the plant operates fully according to the cash flow above. At the end of the plant life, the equipment is assumed to have no salvage value. The working capital and land value is recovered however, at \$75,949,000 and \$26,346,000 respectively. The cumulative discounted cash flow is calculated at a minimum acceptable return of 10% per year.

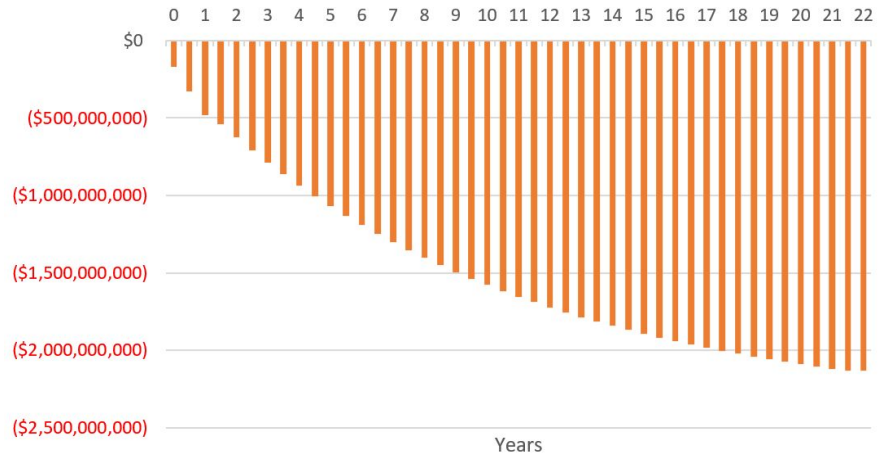


Figure 5-2-01: Cumulative Discounted Cash Flow

5.3 Scenarios

5.3.1 Increased Fuel Prices

The simplest scenario which could mitigate the losses is assuming that the biofuel prices would be higher than they are currently. Alternatively, the selling prices could be higher in the future due to government subsidies for biofuel. It was found that in order to be a feasible investment, breaking even in cumulative cash flow in the plant's lifespan, the price of ethanol and biodiesel would have to be 6.4 times greater than present. This corresponds to ethanol selling for \$5.95 per gallon and biodiesel for \$23.80 per gallon.

In this scenario, the yearly post-tax income of the plant becomes \$32,793,000. This corresponds to an internal rate of return of 10%, our discount rate. The cumulative discounted cash flow diagram for this scenario is shown in Figure 5-3-01. Ultimately these prices or subsidies cannot realistically be expected to occur in the near future, so other scenarios should be considered.

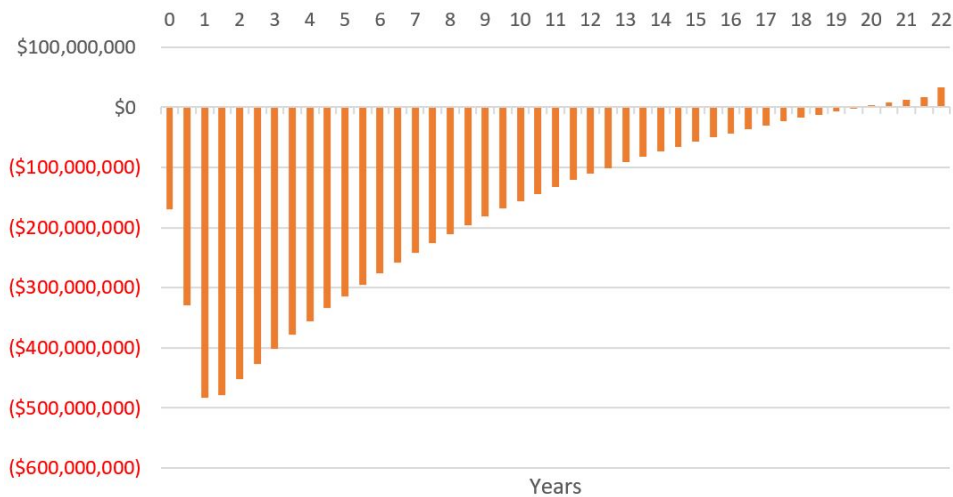


Figure 5-3-01: Cumulative Discounted Cash Flow at Higher Fuel Prices

5.3.2 Better Algae Growth

One of the largest drawbacks of the current design is the large amounts of lands and water it requires. An increased cell harvesting density could allow us to keep the same amount of product, while adjusting the scale of the algae cultivation and harvesting processes, which accounts for around 50% of the capital and 24% of operating costs. If the cell harvesting density could somehow be increased to 0.5 g/L, while keeping the cultivation period the same, a decrease in cultivation land, mixer, and sedimentation tanks to around 44% the current capacity would be observed. Assuming that all these processes did half in size, the facility would see a decrease in capital cost by approximately 24% and in operating costs by 12%. However, this change also is not enough to result in a net operating gain. Significantly faster growing and higher cell densities of algae is necessary to make this process profitable.

5.3.3 Multiple Effect Evaporation

Multiple-effect evaporation is often used, recovering the evaporated steam from one effect to heat the next. The tradeoff in deciding how many effects to use is the decreased operating cost for steam versus the increased capital cost for the number of effects. For this purpose, the steam usage is assumed to scale inversely with the number of effects, while the capital cost increases proportionally with the number of effects (McCabe et al., 2005).

To decide if an incremental change is worth investment, the return on investment (yearly savings divided by initial cost) of the change must exceed 15%. The savings and costs of increasing the number of effects is summarized in Table 5-3-01. The investment is the fixed capital cost for the equipment. Fixed charges are 3% of investment, for property tax and

insurance, plus \$67,000 for labor which is assumed constant. Income tax is neglected, assuming the total income is less than depreciation.

Table 5-3-01: Number of Evaporator Effects Return on Investment (ROI)

# of Effects	Steam (\$/yr)	Investment (\$)	Fixed Costs (\$/yr)	Total Costs (\$/yr)	ROI (%)
1	35,032,000	59,118,000	1,841,000	36,873,000	-
2	17,516,000	118,236,000	3,614,000	21,130,000	26.6
3	11,677,000	177,355,000	5,388,000	17,065,000	6.9
4	8,758,000	236,473,000	7,161,000	15,919,000	1.9
5	7,006,000	295,591,000	8,935,000	15,941,000	-0.04

Two effects is optimal for the current design, halving the steam consumption while doubling the capital investment. When placed in the context of the whole plant, this changes the cashflow to be a loss of \$89,551,000 per year, increases the total capital cost to \$575,880,000, and reduces the break-even fuel prices to 5.9 times the current prices, at \$5.49 per gallon and \$21.95 per gallon for ethanol and biodiesel respectively.

The capital investment cost and fixed operating costs for the evaporators grow to be very large, limiting the return on investment of increasing the number of effects. The largest reason for this is having duplicate evaporators for scaling removal, and building the evaporators of stainless steel to prevent ferric chloride corrosion, both of which about double the cost of evaporators. Anti-scaling coatings or additives can reduce the first factor, although additives must be safe to yeast. When the capital cost is halved, three effects is optimal; when it is quartered, four effects is optimal.

5.3.4 Glycerol and Gypsum Side Products

Glycerol and gypsum are disposed of as waste streams in the design. However, their purity is not very far from acceptable. The glycerol waste is 94% glycerol with the balance ethanol and water, while the gypsum waste is 50% gypsum, or 88% without water, with the balance algae waste. For this hypothetical, we assume these streams can be sold at half market price to nearby plants to perform the necessary distillation, washing, and drying needed.

Table 5-3-02: Product Revenue with Side Products

Product	Amount Produced	Price	Income (\$/yr)
Ethanol	2,968,430 gal/yr	0.93 \$/gal	2,761,000
Diesel	6,132,000 gal/yr	3.72 \$/gal	22,811,000
Gypsum	126,000 ton/yr	150 \$/ton	18,900,000
Glycerol	1,790 ton/yr	350 \$/ton	626,500
Total			45,099,000

In this case, the gypsum disposal cost of \$9,085,000/yr is eliminated as well. In this scenario, the post-tax cashflow comes to be a loss of \$76,682,000/yr. This requires an increase of fuel prices by 5.2 times for a positive net present value, or \$4.84/gallon for ethanol and \$19.34/gallon for biodiesel. Most of the additional revenue comes from the gypsum, which nearly doubles the revenue at current prices. This scenario doesn't consider transportation costs, which can be significant to handle the gypsum cake.

Combining this scenario with the multiple-effect evaporation, the cashflow becomes a loss of \$60,940,000/yr with a capital cost of \$575,880,000. To be a positive investment, fuel prices must be 4.8 times higher, at \$4.46/gallon for ethanol and \$17.86/gallon for biodiesel.

Without major changes in design, this is near a minimum bound for fuel prices that can make the investment feasible.

5.3.5 Avoiding Neutralization and Evaporation

Considering the large capital cost of evaporators and filters, and the operating costs of steam and the acid-base chemistry needed for fermentation, it is desirable to avoid these costs. One way this may be done is through heterogeneous rather than homogeneous catalysts. Research has been done into solid-acid catalysts performing acid hydrolysis to produce glucose from cellulose (Huang & Fu, 2013; Onda et al., 2008), although it isn't clear if such catalysts can similarly prepare lipids for hexane extraction. For the purposes of this analysis, it is assumed no extra steps would be needed to prepare lipids for extraction. With a heterogeneous catalyst, operating costs from acid-base feedstocks, gypsum disposal, neutralization, and filtration are eliminated. Similarly, capital costs for neutralization and filtration are eliminated, and evaporation capital cost is reduced since the fluid is no longer a slurry.

To avoid evaporation, more water may be removed during sedimentation. Sedimentation as designed can bring the algae to 70 g/L, over the current 20 g/L (Bux, 2013). This reduces the amount of water by about 5/7ths, or 71%. Ho et al. (2013) found lower conversions to glucose at this concentration, near 85%, although this is still with homogeneous acid and the same residence time as lower concentrations. Park et al. (2014) did not test at any other algae concentrations. More research would be needed to produce an accurate design at this higher concentration. An estimate will be made at the same conversion as the current design.

In the Acid Hydrolysis step, the sulfuric acid feed is removed and solid acid catalyst must be purchased. Changes in residence time approximately cancel out for the reactor: the reduction in volume flow to 29% of original is about equal to the increased velocity in a 30%-porosity packed bed, so the reactor size is the same. The solid acid catalyst is assumed to be Amberlyst resin to estimate cost, at \$2000/m³ on Alibaba. For the 155 m³ reactor, this is an extra \$310,000 purchase cost or about \$1,838,000 fixed capital cost for the catalyst. The acid storage tank may be eliminated, at \$1,036,000 purchase cost or \$6,143,000 capital cost. The steam consumption to heat the feed may also be reduced by 71%.

The operating and capital costs of neutralization and filtration are eliminated. The current design evaporates 9,601,200 kg of water per day, however with 2/7ths of the water entering and no filtration wash adding water, about 1,700,000 kg of water per day or 18% of the current amount must be removed. A single, four-effect evaporator of the same design is used; duplicates are not needed without the scaling of gypsum. Thus the capital cost is two-thirds of the evaporator in the original design, and steam cost is taken as 4.5% of the original design (18% times 25%). Approximate capital cost changes are summarized in Table 5-3-02, and approximate operating cost reductions are summarized in Table 5-3-03.

Table 5-3-03: Change in Total Capital Costs in Solid Acid Catalyst Scenario

Item	Cost/Cost Change (\$)
Design Cost	506,251,000
Algae Pretreatment	-4,305,000
Neutralization	-2,715,000
Evaporation	-23,186,000
Filtration	-65,600,000
Scenario Cost	410,445,000

Table 5-3-04: Change in Operating Costs in Solid Acid Catalyst Scenario

Item	Cost/Cost Change (\$/year)
Design Operating Cost	107,068,000
Algae Pretreatment	-14,967,000
Neutralization	-5,487,000
Evaporation	-36,919,000
Filtration	-9,159,000
Scenario Cost	40,536,000

In this scenario, the insurance and property tax costs reduce by \$2,874,000 per year with the fixed capital. Even with these reductions, the total yearly cash flow is a negative \$36,319,000. The break-even prices for fuels, however, are lower at 3.4 times the current prices, or \$3.16/gal and \$12.65/gal for ethanol and biodiesel respectively. The opportunity for significant reduction in operating costs is clear, thus we recommend a detailed design with solid acid catalysts, should the data be available, and higher concentration via sedimentation.

5.3.6 Eliminating Ethanol Production

Considering the low proportion of revenue from ethanol, eliminating the ethanol production portion of the plant may improve the overall profitability of the plant. As designed, the ethanol portions of the plant compose about 38% of capital cost and 53% of operating costs for 11% of the revenue.

With the large amount of sulfuric acid-algae mixture leaving lipid extraction, waste disposal can still remain a major cost without any ethanol production. This stream can be neutralized with sodium hydroxide instead of calcium hydroxide, since the stream is no longer

fed to yeast. The cost for 29,620 tons per year of sodium hydroxide at \$50 per ton (per Alibaba) is \$1,481,000 per year. In the best case, this 11,212,400 kg/day salt-water algae waste stream can be disposed of as wastewater at \$0.53 per ton (Peters et al., 2003), which results in a yearly cost of \$2,169,000. The results of eliminating ethanol costs, other than neutralization, are summarized in Tables 5-3-04 and 5-3-05.

Table 5-3-05: Change in Total Capital Costs with Ethanol Elimination

Item	Cost/Cost Change (\$)
Design Cost	506,251,000
Fermentation Pretreatment	-137,254,000
Ethanol Production	-52,666,000
Scenario Cost	316,331,000

Table 5-3-06: Change in Operating Costs with Ethanol Elimination

Item	Cost/Cost Change (\$/year)
Design Operating Cost	107,068,000
Fermentation Pretreatment	-54,558,000
Ethanol Production	-2,451,000
Neutralization and Disposal	3,650,000
Scenario Cost	53,709,000

In cash flow, there is also a reduction of \$5,698,000 per year in insurance and property tax, as well as the \$2,761,000 per year reduction in revenue. In this scenario, the breakeven price for diesel is 4.1 times the current price, at \$15.25 per gallon. Since this breakeven price is lower than the current design or that of multiple-effect evaporation, ethanol production as designed does not improve the profitability of the plant as long as disposal of the waste stream does not

become a large expense. Still, since this breakeven price is higher than that of the solid-acid catalyst scenario (Section 5.3.5), ethanol production can still be profitable in other designs.

6. Safety, Health, Environmental, and Social Considerations

6.1 Health and Safety Considerations

The primary safety concern for acid hydrolysis is the use of large amounts of concentrated sulfuric acid. Sulfuric acid is toxic and corrosive. Leaks pose a serious safety risk, whether of acid alone or the algae-acid mixture. The reactor is under pressure and above the solution's boiling point, so leaks could vaporize causing burns or inhalation of sulfuric acid. The heated section can be easily physically isolated to mitigate this risk. Large amounts of acid may be stored at any time, thus the tanks should be a safe distance from potential sources of vaporization or reaction.

Ethanol is the most volatile component in the process, which can become an asphyxiant when leaks or fires release vapors. Inhalation can cause alcohol poisoning if the victim does not immediately head to a ventilated area. Denaturant is not added in the process, so ingestion or skin contact is not toxic.

Fires can become significant risks, particularly around the ethanol and biodiesel production. Proper safety relief valves feeding to large enough flares or incinerators should mitigate this risk in most emergencies. Product storage should be minimized as much as possible to reduce the size and safety risk of fires.

This process uses many large vessels that will need to be maintained regularly, such as the neutralization reactor to remove scaling. During maintenance, asphyxiation can become a risk in enclosed spaces. In these cases, ventilation must be ensured and workers closely monitored while performing maintenance.

There are other non-chemical risks present in the design. The process will contain pipes and vessels carrying high temperature fluids, so care will need to be taken to ensure that workers don't come into contact with these. This will involve warnings around dangerous areas and insulation. There are other mechanical risks. The plant will likely require a railyard to receive feedstocks and deliver products, which will require worker protocol to minimize danger around the trains and their cars.

Safety concerns for the algae farms primarily include the hazard of falling into the algae ponds. While the algae ponds are shallow, the large amounts of pond area poses the risk of carts or people falling into the ponds. The risk increases further for children.

6.2 Environmental Considerations

There are many environmental considerations associated with the algae biorefinery design, such as providing a renewable energy source and nitrogen removal for wastewater facilities. Algae is a carbon neutral plant, meaning that it does not contribute to increased levels of carbon dioxide and could be a green alternative to other fuels. With the current facility, 220,000 kilograms of algae per day are produced. Each kilogram of algae has the capacity to absorb 1.83 kilograms of CO₂ (Anguselvi et al., 2019). From these values, approximately 147,000 tons of CO₂ is absorbed yearly through algae growth.

Ethanol and diesel productions are at 3,961,000 and 6,132,000 gallons per year, respectively. When converted into mass terms, the ethanol production is approximately 12,000,000 kg/year and diesel is 20,000,000 kg/year. Assuming complete combustion of each product annually with no impurities or any other outside influences, approximately 98,000 tons

of CO₂ are produced. Therefore, growing and processing the algae yields a carbon sink of 49,000 tons of CO₂ yearly, largely from unused algal proteins.

Combusting 1 kilogram of ethanol produces 26.2 megajoules. Over the course of one calendar year with current productions, this yields 315,000,000 MJ of energy per year.

Combusting 1 kilogram of biodiesel produces 37.8 MJ, which becomes 756,000,000 MJ of energy per year. Combining the ethanol and diesel energy output yields a total energy production per year of 1,071,000 GJ.

The plant currently requires an energy input of approximately 1,446,000 GJ/year to operate. This is greater than the energy produced in the output biodiesel and ethanol, so from purely an energy perspective this plant is not efficient.

Another significant environmental consideration of the plant is that it would allow for nitrogen removal from wastewater, something that wastewater facilities struggle to do. Nitrogen in wastewater often results in algae blooms, which is something that our facility hopes to do and run off but is undesirable for wastewater facilities. The incoming wastewater will have around 50 mg/L of nitrogen. We expect to send 99% of this water back to the wastewater facility after algae harvesting, having removed at least around 95% of the nitrogen. Further, the wastewater dispelled after algae harvesting will have around 0.002 wt% ferric chloride. Ferric chloride is often used as a coagulant in wastewater facilities, as it is an efficient coagulant and useful as a sludge dewatering agent. The incoming wastewater with the coagulant is thus likely desirable for wastewater facilities. In the worst case scenario, wastewater treatment facilities use a different coagulant.

Sulfuric acid may enter the environment in cases of leaks, fires, separation errors downstream, or other emergencies. Sulfuric acid and related sulfur emissions create acid rain, which has ill effects on the health of aquatic wildlife and trees. Sulfuric acid is a common industrial catalyst, so the market easily accommodates increased demand, however use does contribute to environmental impacts of production and delivery.

Gypsum is widely used in construction and even used in food products like tofu, and thus taken as safe to dispose of in a landfill. The gypsum is not sold as a side-product due to an unknown amount of algae waste, primarily proteins and unextracted lipids, remaining in the cake. In a landfill, glucose and algae waste may be leached from the gypsum cake, possibly affecting groundwater and local flora. At worst, the nutrients may cause minor algae blooms downstream, similar to fertilizers. The amounts of each element in the cake are estimated to be relatively low, although there is uncertainty without filtration data.

Additionally, there are two waste streams coming from biodiesel purification. One is 96% glycerol, 2.8% ethanol, 0.6% water, 0.2% biodiesel/oil coming from the gravity settler, and the other is 49.7% biodiesel, 34.1% ethanol, 15.5% glycerol, and 0.7% water coming from the secondary flash on the biodiesel phase after the settler. The glycerol waste stream is likely pure enough that it could be used or sold as is (this use hasn't been priced into economics), such as being fed back into the algae or sold as an additive to animal feed due to its low toxicity (Yang et al., 2012). The other stream is fairly impure but relatively flammable and low volume in terms of production, so it would likely be simplest to just burn it off. This would have no more carbon impact than if it was used as fuel anyway, so the only downside to this is a small loss of product (~1.5% of biodiesel production).

6.3 Social Considerations

There are many positive and negative social impacts and consideration of building this facility. This facility would create over a hundred jobs for rural Texas, for farmers, engineers and operators, and provide a renewable energy source. The facility would be selling around 3M gallons/year of ethanol and 6M gallons/year of biodiesel. In 2019, the US produced around 16B gallons of ethanol and 2.5B gallons of biodiesel (McCaherty et al., n.d.; U.S. Energy Information Administration, 2019a). The US imported around 168M gallons of biodiesel in 2019, and while the amount of biodiesel produced is only around 3.5 percent of that, it will be contributing to reduced dependence on foreign countries for biodiesel. The US is one of the largest exporters of ethanol so the ethanol produced makes less of a difference in terms of overall production.

Overall, the amount of fuels produced are minor enough to not disrupt the market.

As mentioned earlier, the factory creates a lot of jobs in rural Texas. However, workers would likely have to commute into work from places that are far, which could result in more travel pollution and take up a lot of time for the workers. Modes of public transportation, such as buses, may also be used to make commuting more reasonable and environmentally friendly.

The algae farm would also take up a lot of space, requiring it to be far away from any residential areas. The large amounts of farm that would be used for algae cultivation could also be used for other purposes. Further, the cultivation farm would be smelly, making it an unpleasant place to work at or live near.

7. Conclusions and Recommendations

With the current fuel prices and the costs of production, we cannot reasonably recommend the plant is built at this time. Conceptually, a biofuels facility would be an excellent alternative to fossil fuels, but the current feedstock technology does not support a lucrative large scale manufacturing.

Better algae cultivation and harvesting technology is desirable as a significant downfall of the current design is the large amounts of land and water that is involved in the process. While open pond raceways are cheaper to construct than photobioreactors, the biomass productivity is much lower. Further, while cultivating the algae in a batch configuration with nutrient depletion allowed for an increased percentage of lipids in algae, it resulted in slower algae growth towards the end of cultivation and hindered the use of techniques such as dilution to allow for increased biomass production. A feedstock that is richer in nitrogen is also recommended as an increased nitrogen content allows for better algae growth. Another limiting factor for algae growth was light attenuation, because of which harvesting cell densities must be kept low. At this time, a faster growing algae strain and technology to minimize light attenuation issues in raceways are needed to make algae biofuel plants more economical.

Preparing the glucose stream for fermentation is one of the most significant costs. Two-effect evaporation is slightly more cost efficient, although the high cost of evaporators limits improvement. The costs of acid-base feedstocks and disposal are also significant. If a solid acid catalyst is used and more water is removed initially, the plant can reduce total yearly costs by 56% and capital costs 18%. This is in lack of design data, and still results in an economic loss. It may provide a basis for future designs, however.

Overall, this plant would result in many positives for the community, such as creating jobs, lowering fossil fuel dependence, and partially treating wastewater. However, we cannot overlook the problems associated with the facility, including copious amounts of land, lack of economic incentive, and net energy loss.

8. Acknowledgements

We would like to thank Professor Eric Anderson for his crucial help throughout the year, in topics ranging from research to design and economics. Additionally, we would like to thank Professor George Prpich for his open doors, advice and help whenever it was needed.

9. References

- 2020 Costs to Build a Pond | Prices to Dig a Koi Pond, Lake—HomeAdvisor. (n.d.). Retrieved April 6, 2020, from <https://www.homeadvisor.com/cost/landscape/install-a-pond/>
- Adesanya, V. O., Vadillo, D. C., & Mackley, M. R. (2012). The rheological characterization of algae suspensions for the production of biofuels. *Journal of Rheology*, *56*(4), 925–939. <https://doi.org/10.1122/1.4717494>
- Ajanovic, A. (2011). Biofuels versus food production: Does biofuels production increase food prices? *Energy*, *36*(4), 2070–2076. <https://doi.org/10.1016/j.energy.2010.05.019>
- Alameda, M., Bumila, K., Carino, I., & McIninch, G. (2015). *Removing Water from an Azeotropic Ethanol-Water Mixture through Adsorption*. 72.
- Amini, H., Wang, L., Hashemsohi, A., Shahbazi, A., Bikdash, M., Kc, D., & Yuan, W. (2018). An integrated growth kinetics and computational fluid dynamics model for the analysis of algal productivity in open raceway ponds. *Computers and Electronics in Agriculture*, *145*, 363–372. <https://doi.org/10.1016/j.compag.2018.01.010>
- Amini, H., Wang, L., & Shahbazi, A. (2016). Effects of harvesting cell density, medium depth and environmental factors on biomass and lipid productivities of *Chlorella vulgaris* grown in swine wastewater. *Chemical Engineering Science*, *152*, 403–412. <https://doi.org/10.1016/j.ces.2016.06.025>
- Anderson, E. (2020, February). *Anderson Distillation Recommendation* [Verbal].
- Anguselvi, V., Masto, R. E., Mukherjee, A., & Singh, P. K. (2019). CO₂ Capture for Industries by Algae. *Algae*. <https://doi.org/10.5772/intechopen.81800>
- Biello, D. (2013, July 25). *How to survive as a biofuel-maker: Sell algae to bakers*. Scientific

American.

<https://www.scientificamerican.com/article/how-to-survive-as-former-algae-biofuel-maker-solazyme/>

Budz, J., Jones, A. G., & Mullin, J. W. (2007). Effect of selected impurities on the continuous precipitation of calcium sulphate (gypsum). *Journal of Chemical Technology & Biotechnology*, 36(4), 153–161. <https://doi.org/10.1002/jctb.280360402>

Bux, F. (Ed.). (2013). *Biotechnological applications of microalgae: Biodiesel and value added products*. CRC Press, Taylor & Francis Group.

Chatsungnoen, T., & Chisti, Y. (2016). Harvesting microalgae by flocculation–sedimentation. *Algal Research*, 13, 271–283. <https://doi.org/10.1016/j.algal.2015.12.009>

Chisti, Y. (2007). Biodiesel from microalgae. *Biotechnology Advances*, 25(3), 294–306. <https://doi.org/10.1016/j.biotechadv.2007.02.001>

Chisti, Y. (2013). Raceways-based Production of Algal Crude Oil. *Green*, 3(3–4). <https://doi.org/10.1515/green-2013-0018>

Chisti, Y. (2016). Large-Scale Production of Algal Biomass: Raceway Ponds. In Faizal Bux & Y. Chisti (Eds.), *Algae Biotechnology* (pp. 21–40). Springer International Publishing. https://doi.org/10.1007/978-3-319-12334-9_2

Clifford, C. B. (n.d.). 9.3 Various Processes Used to Make Biodiesel | EGEE 439: Alternative Fuels from Biomass Sources. Pennsylvania State University. Retrieved April 5, 2020, from <https://www.e-education.psu.edu/egee439/node/685>

Comesaña, J. F., Otero, J. J., García, E., & Correa, A. (2003). Densities and Viscosities of Ternary Systems of Water + Glucose + Sodium Chloride at Several Temperatures.

- Journal of Chemical & Engineering Data*, 48(2), 362–366.
<https://doi.org/10.1021/je020153x>
- Converti, A., Casazza, A. A., Ortiz, E. Y., Perego, P., & Del Borghi, M. (2009). Effect of temperature and nitrogen concentration on the growth and lipid content of *Nannochloropsis oculata* and *Chlorella vulgaris* for biodiesel production. *Chemical Engineering and Processing: Process Intensification*, 48(6), 1146–1151.
<https://doi.org/10.1016/j.cep.2009.03.006>
- Dassey, A. J., & Theegala, C. S. (2013). Harvesting economics and strategies using centrifugation for cost effective separation of microalgae cells for biodiesel applications. *Bioresource Technology*, 128, 241–245. <https://doi.org/10.1016/j.biortech.2012.10.061>
- Dauta, A., Devaux, J., Piquemal, F., & Boumnick, L. (1990). Growth rate of four freshwater algae in relation to light and temperature. *Hydrobiologia*, 207(1), 221–226.
<https://doi.org/10.1007/BF00041459>
- Davis, R., Aden, A., & Pienkos, P. T. (2011). Techno-economic analysis of autotrophic microalgae for fuel production. *Applied Energy*, 88(10), 3524–3531.
<https://doi.org/10.1016/j.apenergy.2011.04.018>
- De Bhowmick, G., Sarmah, A. K., & Sen, R. (2019). Zero-waste algal biorefinery for bioenergy and biochar: A green leap towards achieving energy and environmental sustainability. *Science of The Total Environment*, 650, 2467–2482.
<https://doi.org/10.1016/j.scitotenv.2018.10.002>
- Deshpande, S. R., Sunol, A. K., & Philippidis, G. (2017). Status and prospects of supercritical alcohol transesterification for biodiesel production: Supercritical alcohol

- transesterification for biodiesel production. *Wiley Interdisciplinary Reviews: Energy and Environment*, 6(5), e252. <https://doi.org/10.1002/wene.252>
- Eastman Chemical Company. (2015). *Therminol 68: Heat transfer fluid*.
- Gnansounou, E., & Kenthorai Raman, J. (2016). Life cycle assessment of algae biodiesel and its co-products. *Applied Energy*, 161, 300–308.
<https://doi.org/10.1016/j.apenergy.2015.10.043>
- Gomiero, T. (2015). Are biofuels an effective and viable energy strategy for industrialized societies? A reasoned overview of potentials and limits. *Sustainability*, 7(7), 8491–8521.
<https://doi.org/10.3390/su7078491>
- Gominšek, T., Lubej, A., & Pohar, C. (2005). Continuous precipitation of calcium sulfate dihydrate from waste sulfuric acid and lime. *Journal of Chemical Technology & Biotechnology*, 80(8), 939–947. <https://doi.org/10.1002/jctb.1266>
- Gurgel, L. V. A., Marabezi, K., Zambom, M. D., & Curvelo, A. A. da S. (2012). Dilute Acid Hydrolysis of Sugar Cane Bagasse at High Temperatures: A Kinetic Study of Cellulose Saccharification and Glucose Decomposition. Part I: Sulfuric Acid as the Catalyst. *Industrial & Engineering Chemistry Research*, 51(3), 1173–1185.
<https://doi.org/10.1021/ie2025739>
- Hannon, M., Gimpel, J., Tran, M., Rasala, B., & Mayfield, S. (2010). Biofuels from algae: Challenges and potential. *Biofuels*, 1(5), 763–784.
- Ho, S.-H., Huang, S.-W., Chen, C.-Y., Hasunuma, T., Kondo, A., & Chang, J.-S. (2013). Bioethanol production using carbohydrate-rich microalgae biomass as feedstock. *Bioresource Technology*, 135, 191–198. <https://doi.org/10.1016/j.biortech.2012.10.015>

Houston TX Average Temperatures by Month—Current Results. (n.d.). Retrieved April 6, 2020,
from

<https://www.currentresults.com/Weather/Texas/Places/houston-temperatures-by-month-average.php>

Huang, Y.-B., & Fu, Y. (2013). Hydrolysis of cellulose to glucose by solid acid catalysts. *Green Chemistry*, 15(5), 1095–1111. <https://doi.org/10.1039/C3GC40136G>

Jääskeläinen, H. (2009). *Biodiesel standards and properties*. [Online] January 1, 2009. [Cited: November 2, 2009.].

Katzen, R., Madson, P. W., & Moon, G. D. (n.d.). *Ethanol distillation: The fundamentals*. 20.

Krishnan, M. S., Ho, N. W. Y., & Tsao, G. T. (1999). Fermentation Kinetics of Ethanol Production from Glucose and Xylose by Recombinant *Saccharomyces* 1400(pLNH33). *Applied Biochemistry and Biotechnology*, 77, 17.

Kunihisa, K. S., & Ogawa, H. (1985). Acid hydrolysis of cellulose in a differential scanning calorimeter. *Journal of Thermal Analysis*, 30(1), 49–59.

<https://doi.org/10.1007/BF02128114>

LaMorte, W. W. (2016, March 22). *Lipids*.

http://sphweb.bumc.bu.edu/otlt/MPH-Modules/PH/PH709_BasicCellBiology/PH709_BasicCellBiology4.html

Li, Y., Horsman, M., Wu, N., Lan, C. Q., & Dubois-Calero, N. (2008). Biofuels from microalgae. *Biotechnology Progress*, 24(4), 815–820. <https://doi.org/10.1021/bp070371k>

Liquid-Liquid Extraction. (2013, October 2). Chemistry LibreTexts.

https://chem.libretexts.org/Bookshelves/Ancillary_Materials/Demos%2C_Techniques%2

- Maiorella, B. L., Blanch, H. W., & Wilke, C. R. (1984). Feed component inhibition in ethanolic fermentation by *Saccharomyces cerevisiae*. *Biotechnology and Bioengineering*, *26*(10), 1155–1166. <https://doi.org/10.1002/bit.260261004>
- Martín, M., & Grossmann, I. E. (2013). Optimal engineered algae composition for the integrated simultaneous production of bioethanol and biodiesel. *AIChE Journal*, *59*(8), 2872–2883. <https://doi.org/10.1002/aic.14071>
- McAloon, A., Taylor, F., & Yee, W. (2000). *Determining the Cost of Producing Ethanol from Corn Starch and Lignocellulosic Feedstocks*. 44.
- McCabe, W. L., Smith, J. C., & Harriott, P. (2005). *Unit operations of chemical engineering* (7th ed). McGraw-Hill.
- McCaherty, J., Wilson, C., & Cooper, G. (n.d.). *2019 Ethanol Production Outlook*. 36.
- McCall, M. T., & Tadros, M. E. (1980). Effects of additives on morphology of precipitated calcium sulfate and calcium sulfite—Implications on slurry properties. *Colloids and Surfaces*, *1*(2), 161–172. [https://doi.org/10.1016/0166-6622\(80\)80003-5](https://doi.org/10.1016/0166-6622(80)80003-5)
- Mujtaba, G., Choi, W., Lee, C.-G., & Lee, K. (2012). Lipid production by *Chlorella vulgaris* after a shift from nutrient-rich to nitrogen starvation conditions. *Bioresource Technology*, *123*, 279–283. <https://doi.org/10.1016/j.biortech.2012.07.057>
- Nan, Y., Liu, J., Lin, R., & Tavlarides, L. L. (2015). Production of biodiesel from microalgae oil (*Chlorella protothecoides*) by non-catalytic transesterification in supercritical methanol and ethanol: Process optimization. *The Journal of Supercritical Fluids*, *97*, 174–182. <https://doi.org/10.1016/j.supflu.2014.08.025>

- Nancollas, G. H., Reddy, M. M., & Tsai, F. (1973). Calcium sulfate dihydrate crystal growth in aqueous solution at elevated temperatures. *Journal of Crystal Growth*, *20*(2), 125–134. [https://doi.org/10.1016/0022-0248\(73\)90126-7](https://doi.org/10.1016/0022-0248(73)90126-7)
- Onda, A., Ochi, T., & Yanagisawa, K. (2008). Selective hydrolysis of cellulose into glucose over solid acid catalysts. *Green Chemistry*, *10*(10), 1033. <https://doi.org/10.1039/b808471h>
- Park, J.-Y., Oh, Y.-K., Lee, J.-S., Lee, K., Jeong, M.-J., & Choi, S.-A. (2014). Acid-catalyzed hot-water extraction of lipids from *Chlorella vulgaris*. *Bioresource Technology*, *153*, 408–412. <https://doi.org/10.1016/j.biortech.2013.12.065>
- Park, J.-Y., Park, M. S., Lee, Y.-C., & Yang, J.-W. (2015). Advances in direct transesterification of algal oils from wet biomass. *Bioresource Technology*, *184*, 267–275. <https://doi.org/10.1016/j.biortech.2014.10.089>
- Patle, D. S., Wei, P. E., & Ahmad, Z. (2015). Simulation and Economic Analysis of Biodiesel production using Supercritical Methanol. *Journal of Engineering Science*, *11*, 10.
- Peters, M. S., Timmerhaus, K. D., & West, R. E. (2003). *Plant design and economics for chemical engineers* (5th ed). McGraw-Hill.
- Pilath, H. M., Nimlos, M. R., Mittal, A., Himmel, M. E., & Johnson, D. K. (2010). Glucose Reversion Reaction Kinetics. *Journal of Agricultural and Food Chemistry*, *58*(10), 6131–6140. <https://doi.org/10.1021/jf903598w>
- Příbyl, P., Cepák, V., & Zachleder, V. (2012). Production of lipids in 10 strains of *Chlorella* and *Parachlorella*, and enhanced lipid productivity in *Chlorella vulgaris*. *Applied Microbiology and Biotechnology*, *94*(2), 549–561. <https://doi.org/10.1007/s00253-012-3915-5>

- PubChem. (n.d.). *Triolein*. Retrieved March 22, 2020, from
<https://pubchem.ncbi.nlm.nih.gov/compound/5497163>
- Richards, O. W. (1925). THE EFFECT OF CALCIUM SULFATE ON THE GROWTH AND FERMENTATION OF YEAST ¹. *Journal of the American Chemical Society*, 47(6), 1671–1676. <https://doi.org/10.1021/ja01683a023>
- Rostami, M., Raeissi, S., Mahmoodi, M., & Nowroozi, M. (2012). Liquid–Liquid Equilibria in Biodiesel Production. *Journal of the American Oil Chemists' Society*, 90.
<https://doi.org/10.1007/s11746-012-2144-5>
- Saad, M. G., Dosoky, N. S., Zoromba, M. S., & Shafik, H. M. (2019). Algal Biofuels: Current Status and Key Challenges. *Energies*, 12(10), 1920. <https://doi.org/10.3390/en12101920>
- Santana, H. S., Tortola, D. S., Reis, É. M., Silva, J. L., & Taranto, O. P. (2016). Transesterification reaction of sunflower oil and ethanol for biodiesel synthesis in microchannel reactor: Experimental and simulation studies. *Chemical Engineering Journal*, 302, 752–762. <https://doi.org/10.1016/j.cej.2016.05.122>
- Singh, A., Nigam, P. S., & Murphy, J. D. (2011). Mechanism and challenges in commercialisation of algal biofuels. *Bioresource Technology*, 102(1), 26–34.
<https://doi.org/10.1016/j.biortech.2010.06.057>
- Smith, B. R., & Sweett, F. (1971). The crystallization of calcium sulfate dihydrate. *Journal of Colloid and Interface Science*, 37(3), 612–618.
[https://doi.org/10.1016/0021-9797\(71\)90339-0](https://doi.org/10.1016/0021-9797(71)90339-0)
- Sutherland, D. L., Park, J., Heubeck, S., Ralph, P. J., & Craggs, R. J. (2020). Size matters – Microalgae production and nutrient removal in wastewater treatment high rate algal

- ponds of three different sizes. *Algal Research*, 45, 101734.
<https://doi.org/10.1016/j.algal.2019.101734>
- Sutherland, D. L., Turnbull, M. H., & Craggs, R. J. (2014). Increased pond depth improves algal productivity and nutrient removal in wastewater treatment high rate algal ponds. *Water Research*, 53, 271–281. <https://doi.org/10.1016/j.watres.2014.01.025>
- Tripathi, R., Gupta, A., & Thakur, I. S. (2019). An integrated approach for phycoremediation of wastewater and sustainable biodiesel production by green microalgae, *Scenedesmus* sp. ISTGA1. *Renewable Energy*, 135, 617–625. <https://doi.org/10.1016/j.renene.2018.12.056>
- Turton, R. (Ed.). (2018). *Analysis, synthesis, and design of chemical processes* (5th edition). Prentice Hall.
- U.S. Department of Energy. (2018). *Alternative Fuels Data Center: E85 Flex Fuel Specification*.
https://afdc.energy.gov/fuels/ethanol_e85_specs.html
- U.S. Energy Information Administration. (2019a, September 16). *U.S. biodiesel production capacity data—Today in Energy*.
<https://www.eia.gov/todayinenergy/detail.php?id=41314>
- U.S. Energy Information Administration. (2019b). *Monthly energy review* (pp. 179–180).
<https://www.eia.gov/totalenergy/data/monthly/#renewable>
- U.S. Energy Information Administration. (2019c, October 21). *Gasoline and diesel fuel update*.
<https://www.eia.gov/petroleum/gasdiesel/>
- U.S. Energy Information Administration. (2020, March 31). *Texas Natural Gas Prices*.
https://www.eia.gov/dnav/ng/ng_pri_sum_dcu_STX_a.htm
- Vassilev, S. V., & Vassileva, C. G. (2016). Composition, properties and challenges of algae

- biomass for biofuel application: An overview. *Fuel*, 181, 1–33.
<https://doi.org/10.1016/j.fuel.2016.04.106>
- Vogelbusch. (2018). *Vogelbush MultiCont continuous fermentation designs*. Website.
Vogelbusch Biocommodities.
<https://www.vogelbusch-biocommodities.com/process-units/fermentation/multicont-fermentation/>
- Woertz I., Feffer A., Lundquist T., & Nelson Y. (2009). Algae Grown on Dairy and Municipal Wastewater for Simultaneous Nutrient Removal and Lipid Production for Biofuel Feedstock. *Journal of Environmental Engineering*, 135(11), 1115–1122.
[https://doi.org/10.1061/\(ASCE\)EE.1943-7870.0000129](https://doi.org/10.1061/(ASCE)EE.1943-7870.0000129)
- Wu, J., Graham, L. J., & Mehidi, N. N. (2006). Estimation of agitator flow shear rate. *AIChE Journal*, 52(7), 2323–2332. <https://doi.org/10.1002/aic.10857>
- Yang, F., Hanna, M. A., & Sun, R. (2012). Value-added uses for crude glycerol—A byproduct of biodiesel production. *Biotechnology for Biofuels*, 5(1), 13.
<https://doi.org/10.1186/1754-6834-5-13>
- Yaşar, F., & Altun, Ş. (2018). Biodiesel properties of microalgae (*Chlorella protothecoides*) oil for use in diesel engines. *International Journal of Green Energy*, 15(14–15), 941–946.
<https://doi.org/10.1080/15435075.2018.1529589>
- Zentou, H., Zainal Abidin, Z., Yunus, R., Awang Biak, D., Zouanti, M., & Hassani, A. (2019). Modelling of Molasses Fermentation for Bioethanol Production: A Comparative Investigation of Monod and Andrews Models Accuracy Assessment. *Biomolecules*, 9(8), 308. <https://doi.org/10.3390/biom9080308>

- Zhang, H., Yang, L., Zang, X., Cheng, S., & Zhang, X. (2019). Effect of shear rate on floc characteristics and concentration factors for the harvesting of *Chlorella vulgaris* using coagulation-flocculation-sedimentation. *Science of The Total Environment*, 688, 811–817. <https://doi.org/10.1016/j.scitotenv.2019.06.321>
- Zheng, K., Pan, J.-W., Ye, L., Fu, Y., Peng, H.-Z., Wan, B.-Y., Gu, Q., Bian, H.-W., Han, N., Wang, J.-H., Kang, B., Pan, J.-H., Shao, H.-H., Wang, W.-Z., & Zhu, M.-Y. (2007). Programmed Cell Death-Involved Aluminum Toxicity in Yeast Alleviated by Antiapoptotic Members with Decreased Calcium Signals. *Plant Physiology*, 143(1), 38–49. <https://doi.org/10.1104/pp.106.082495>